

Final Draft
of the original manuscript:

Vivone, G.; Braca, P.; Horstmann, J.:

**Knowledge-Based Multitarget Ship Tracking for HF Surface
Wave Radar Systems**

In: IEEE Transactions on Geoscience and Remote Sensing (2015) IEEE

DOI: 10.1109/TGRS.2014.2388355

Knowledge-Based Multi-Target Tracking via UKF-JPDA Variable Structure IMM Estimator in HF Surface Wave Radar Systems

Gemine Vivone, Paolo Braca, and Jochen Horstmann

Abstract

These last decades spawned a great interest towards low-power High-Frequency (HF) Surface-Wave (SW) radars for ocean remote sensing [1]–[4]. These sensors are also effectiveness long-range early-warning tools in maritime situational awareness applications providing an additional source of information for ship detection and tracking, by virtue of their over-the-horizon coverage capability and continuous-time mode of operation [5]. Unfortunately, they exhibit many shortcomings that need to be taken into account, and proper algorithms need to be exploited to fulfill such limitations [6].

In this paper, we develop a Knowledge-Based (KB) multi-target tracking methodology, which takes advantage of *a priori* information about the ship traffic [7]. This prior information is given by the ship sea lanes and by their related motion models, that constitute the basic building blocks of the Variable Structure Interactive Multiple Model (VS-IMM) procedure [8]. Finally, the KB tracking deals with false alarms and miss detections by using the Joint Probabilistic Data Association (JPDA) rule [9], [10] and with the non-linearities by using the Unscented Kalman Filter (UKF) [11].

The KB-tracking procedure is validated using real data of the experimentation conducted by the NATO Science and Technology Organization - Centre for Maritime Research and Experimentation (STO-CMRE) during the Battlespace Preparation 2009 (BP09) HF-radar campaign in the Ligurian Sea (Mediterranean Sea). The experiment setup included two HFSW radar systems, located in the Palmaria island (gulf of La Spezia) and S. Rossore (close to Pisa).

The system performance is defined in terms of Time-on-Target (ToT), False Alarm Rate (FAR), track fragmentation, and accuracy. A full statistical characterization is provided using one month of data. A significant improvement of the KB-tracking procedure, in terms of system performance, is demonstrated in comparison with the standard approach recently presented in [6]. The main result is that there is an increment of the time-on-target for any fixed value of the false alarm rate. The increment is quite sensible in the region of low false alarm rate where can be over 30% for both the Palmaria and S. Rossore systems. The

G. Vivone and P. Braca are with North Atlantic Treaty Organization (NATO) Science and Technology Organization (STO) Centre for Maritime Research and Experimentation, 19126 La Spezia, Italy. J. Horstmann is with Helmholtz-Zentrum Geesthacht, 21502 Geesthacht, Germany.

E-mails: {vivone,braca}@cmre.nato.int, jochen.horstmann@hzg.de.

KB-tracking exhibits on the average a reduction of the track fragmentation, about 20% and 13% for the system in Palmaria and S. Rossore, respectively.

Index Terms

High-frequency surface-wave radar, target detection, target tracking, knowledge-based tracking, maritime surveillance.

I. INTRODUCTION

The oceans connect nations globally through an interdependent network of economic, financial, social and political relationships. The main statistics are compelling: 70% of the Earth is covered in water; 80% of the world's population lives within 100 miles of the coast; 90% of the world's commerce is seaborne and 75% of that trade passes through a few, vulnerable, canals and international straits. The maritime environment includes trade routes, choke points, ports, and other infrastructure such as pipelines, oil and natural gas platforms and trans-oceanic telecommunications cables [12]. Consequently, the maritime security environment is one of the most important operative scenarios, and surveillance activities are the crux of these activities. Ship traffic monitoring represents one of the biggest challenges (*e.g.* in terms of law enforcement, search and rescue, environmental protection and resource management) and, in the last years, it has led to an intensive research activities in order to exploit existing sensor systems in support of maritime surveillance.

In this domain several monitoring assets can be exploited, from radar technologies to satellite positioning systems. However, it is important to take into consideration that many of these traditional solutions suffer from physical limitations, and only a smart integration of these different and often complementary systems can guarantee satisfiable performance. For instance, while standard microwave radars operate only within line-of-sight (LoS) propagation, with a maximum range of some dozens of kilometers, satellite sensors (*e.g.* synthetic aperture radars [13]) cannot grant a continuous temporal coverage of the region of interest with an adequate level of real-time surveillance.

HFSW radar systems can be convincing cost-effective tools, overcoming many of these limitations. They can provide additional information on the vessel traffic, by virtue of their capability of detecting targets Over-The-Horizon (OTH), their continuous-time coverage and direct target velocity estimation through the Doppler data [5]. Another important characteristic is that very low-power is required to operate a single radar site, about 35 W on average, and low electromagnetic pollution is generated.

HFSW radars work in the 3 – 30 MHz band, with wavelengths between 100 m and 10 m, respectively. In this interval, vertically polarized radio waves have also the ability to propagate as surface waves. Low-power HFSW radar systems have been mainly developed for ocean remote sensing applications, *e.g.* surface currents and sea state mapping, wind extraction,

wave spectra analysis and, recently, tsunami early-warning detection [14]. There are many commercial systems, *e.g.* the Coastal Ocean Dynamics Applications Radar (CODAR), developed at NOAA [1], and the Wellen Radar (WERA), developed at the University of Hamburg [15]. These systems can be found mainly operating from the coast, while only a few experiments have been conducted with shipborne installations.

The idea is to take advantage of the growing number of oceanographic HFSW radars along the coasts also for maritime-surveillance applications. Hence, ship detection and sea-state sensing become two complementary problems [5]. In fact, the presence of clutter is unwelcome as far as we are interested in ship detection, while the presence of ships can limit the extraction of oceanographic parameters [3]. For this reason, in the past years much interest has been focused to develop new spectral models for modeling the return from the sea, with the ultimate goals of both enhancing target detection via clutter-suppression techniques [16], and ocean sensing [2], [4].

Since the system is set up for oceanic parameter estimation, its configuration is not optimal for target detection. This represents a further problem, since the signal environment already includes external noise, different types of clutter and interference, which can significantly degrade the detection performance. Poor range and azimuth resolution compared to microwave radars, high non-linearity in the state/measurement space, significant false alarm rate, due to both sea clutter and man-made/natural interference, and the crowding of the HF-spectrum [15] are all problems to cope with.

Attempts to mitigate these problems have been made by applying state-of-the-art algorithms, *e.g.*, see [6], [17]–[22]. In particular in [6] it is shown how the surveillance performance can be enhanced by combining data from multiple radar stations by using a proper algorithmic strategy. The signal processing chain has been divided in three main blocks: Detection, tracking and fusion. The detection stage is performed using a 3D (range-azimuth-Doppler) Ordered Statistics (OS) Constant False Alarm Rate (CFAR) algorithm [23] developed at the University of Hamburg. The tracking part is based on the popular Joint Probabilistic Data Association (JPDA) rule [9], [10] in combination with the Unscented Kalman Filter (UKF) [11]. The data fusion strategy is developed thanks to the Track-to-Track Association and Fusion (T2T-A/F) paradigm [10].

Analyzing some of the results in [6], [19], notwithstanding the good overall performances assessed, the phenomenon of the track fragmentation is evident. It is mainly due to the lack of target contacts for some periods of time. Possible reasons of this problem are given by the radar synchronization turning off and targets sailing in the Bragg scattering regions, generated by those ocean waves of half the radar wavelength and travelling towards and away from the radar site [15]. The presence of this intense scattering enforces a lower sensibility of the detector in such areas that causes an increase of the clutter intensity at the expense of the target capacity detections.

In the present work we show how it is possible to take advantage of prior information about the ship traffic, demonstrating

that the tracking stage can be enhanced by combining on-line data from the HFSW radar and ship traffic information. This information is expressed by a map of geographical ship sea lanes or routes. We propose a Variable Structure Interactive Multiple Model (VS-IMM) tracking procedure, inspired by the ground tracking literature [8]. See also [7] for an overview about knowledge-based techniques.

In order to reduce the track fragmentation we exploit an existing similarity between the ground target tracking and the ship tracking problems, for instance the target obscuration phenomenon. This is due to different causes: In the ground tracking it could be provoked from the presence of hills or tunnels, which hide the target from the sensors point of view. In the case under study, this effect is present when the radar is turned off to reallocate operative HFSW frequencies, when there is a low signal to clutter ratio (*e.g.* in the Bragg scattering region), and when the target aspect angle exhibits weak signal return. Needless to say that the target obscuration needs to be taken into account in order to reduce the track fragmentation and improve the performances.

The specification of a ship sea lane map can be tabulated including sea lane segments, visibility conditions, and initial/final points of sea lanes. Unlike an off-sea lane target, which is free to move in any direction, the motion of an on-sea lane target is highly constrained. To handle motion along the road, the concept of directionally dependent noise is introduced [8]. The standard motion model assumes that the target can move in any direction and, therefore, uses equal process noise variances in both the x and y directions. This means that for off-sea lane, the motion uncertainties in both directions are equal. For on-sea lane targets, the constraint means more uncertainty along the route than orthogonal to it. Thus the IMM module, representing on-sea lane motion, consists of process noise components along and orthogonal to the route, rather than along x and y directions as in the standard model. Extensive simulations were performed [8] that analyzed different algorithms in the context of ground tracking. The analysis shows that the best performance is obtained using VS-IMM, this was able to handle the on/off-road transitions and the change from one road to another more smoothly than the fixed IMM by anticipating target dynamics. Also, once the target begins to move along a particular road, the VS-IMM, which uses a model matched to the road, yields better course estimate than the fixed IMM, which uses an open field model [7].

Starting from the work in [6], [19]–[22], we show, using simulated scenarios and real data of the experimentation conducted by the NATO Science and Technology Organization - Centre for Maritime Research and Experimentation (STO-CMRE) during the Battlespace Preparation 2009 (BP09) HF-radar campaign in the Ligurian Sea (Mediterranean Sea), improvements in terms of appropriated performance indexes: *i*) the pair Time-on-Target (ToT) and False Alarm Rate (FAR); *ii*) Track fragmentation; *iii*) Root Mean Square Error (RMSE) of the target position and velocity. Tracks and detections are validated or labeled as false using ship reports from the Automatic Identification System (AIS), used as ground truth information. It is well-known

that there are vessels not cooperative, in the sense that they do not provide any AIS reports (*e.g.* fishing boats, warships) and consequently the FAR represents a kind of worst case, see also the discussion in [6].

A significant improvement of the KB-tracking procedure, in terms of system performance, is demonstrated in comparison with the standard approach recently presented in [6]. The main result is that there is an increment of the time-on-target for any fixed value of the false alarm rate. The increment is quite sensible in the region of low false alarm rate where can be over 30% for both the systems in Palmaria and S. Rossore. The KB-tracking exhibits on the average a reduction of the track fragmentation, about 20% and 13% for the system in Palmaria and S. Rossore, respectively.

The outline is as follows. In Sec. II we provide information about the experiment. The proposed knowledge-based target tracking methodology is presented in Sec. III. Experimental results are reported in Sec. IV. In the end, conclusions are drawn in Sec. V.

II. THE HFSW RADAR EXPERIMENT

In this section the description of the experiment is provided. In 2009 the staff of the NATO STO-CMRE installed two WERA HFSW radar systems at the coast of the Ligurian Sea: One on Palmaria Island ($44^{\circ} 2' 30''$ N, $9^{\circ} 50' 36''$ E) and another at San Rossore Park ($43^{\circ} 40' 53''$ N, $10^{\circ} 16' 52''$ E). They were operated between May and December 2009 and acquired data on an operational basis to monitor ocean surface currents and waves. The location and the two radars' fields of view are shown in Fig. 1.

Both systems operated at a frequency of ≈ 12.4 MHz (corresponding to a wavelength of $\lambda \approx 24$ m). Each WERA setup consisted of a decoupled transmitting and receiving antenna arrays. The transmit array consisted of 4 antennas arranged in a rectangular shape, whereas the receive array consisted of 16 antennas along the line perpendicular to the look direction. Electronic control of the arrays was adopted to sweep a 120° angular sector depending on the bandwidth, while Doppler resolution is achieved using Continuous Wave (CW) signals [24].

The system uses a Linearly Frequency-Modulated CW (LFMCW), which is a linear chirp with about 100 kHz bandwidth yielding range resolution between 0.3 and 1.5 km. Surface propagation at sea is guaranteed by vertically polarized HF waves, with frequency in the range $\Omega_0 = 3 - 30$ MHz, and thus a wavelength of $\lambda = 10 - 100$ m. The angles with respect to North of the two array installations were $\phi_1 = 296.2^{\circ}$ and $\phi_2 = 12.0^{\circ}$, respectively.

Data are recorded by each antenna element in complex samples over all the range cells. The remaining 206 s seconds are used to select a new free HFSW channel (between 12.190 and 12.595 MHz) and the available bandwidth according to spectrum crowding. The two systems use the same operating frequency, but the modulating waveforms (sawtooth signal) are orthogonal each other for avoiding coupling interferences.

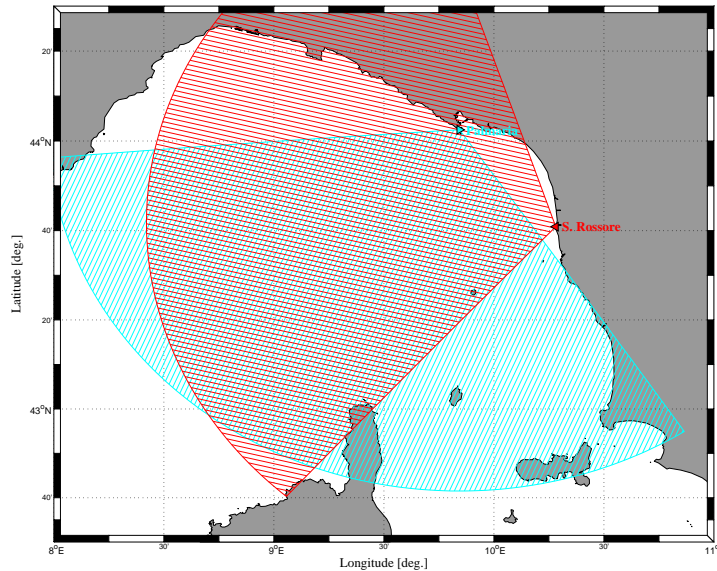


Fig. 1. Setup of the two WERA systems in the Ligurian Sea.

After recording, data from the antennas are beamformed for retrieving azimuth information, then target detection is performed in the Fourier domain by the 3D OS CFAR algorithm [23]. Detection is performed on azimuth cells (1° separated) and the detection statistics are evaluated in the range-Doppler space. An accurate description can be found in [23], [25].

A. The Range-Doppler Space

Taking a look at the HFSW radar spectrum we can observe some peculiarities, see *e.g.* [5]. As far as ship detection is concerned, the contribution of sea clutter is produced by specific spectral components of the surface-height wave-field. The main features are due to the first-order Bragg scattering. They correspond to the advancing (positive frequency shift) and receding (negative frequency shift) ground waves. This phenomenon manifests in the range-Doppler spectrum by means of two lines extending along range, corresponding to the phase-velocities of these scattered ocean waves. However, these frequencies often deviate from the theoretically known values in non-moving waters. In addition, second-order Bragg scattering generates side-band contributions in the range-Doppler spectrum, but are well defined only in the proximity of the radar. Here sea clutter level dominates both targets, noise and interferences. When a vessel is present in this region (*i.e.* has a radial velocity compatible with the Bragg scattering frequency) then it is highly likely to be undetected because of the large sea clutter level. However, this obscuration phenomenon can be corrected (when the vessel is moving on a sea lane) using the KB tracking procedure.

Beyond the sea and land clutter, a variety of interference sources, both natural and man-made, can degrade the reception of

ship echoes. The former type usually consists of large returns (horizontal lines), which cover a large portion of the Doppler space. These interferences are mainly due to unwanted propagation modes through the ionosphere and/or meteor trails echoes. The second type is instead represented by Radio Frequency Interference (RFI). These returns manifest as vertical lines in the range-Doppler spectrum, and can mask both sea clutter and ship echoes.

III. KB TRACKING METHODOLOGY

This section is devoted to the description of the KB tracking procedure applied to the HFSW radar for maritime traffic surveillance. This procedure is an enhanced version of the JPDA-UKF rule [6], [19]–[22] which integrates the VS-IMM mechanism able to take advantage of the prior information about the historical ship traffic. The exploitation of this information in the tracking algorithm is a key ingredient of this work and a brief description of the ship traffic information is provided in the following section.

A. Ship Traffic Information

Ships and vessels exceeding a given gross tonnage¹ are equipped with AIS transponders for position-reporting, as established by the SOLAS Convention [26]. Ships repeatedly broadcast their name, position and other details for automatic display on nearby ships. While this allows ships to be aware and keep track of other ships in their immediate vicinity, coastal states will also be able to receive, plot and log the data by means of base stations along the coast. AIS reports contain both dynamic information (*e.g.* latitude, longitude, Course-Over-Ground (COG), Speed-Over-Ground (SOG), time) and static information (*e.g.* vessel type, dimensions information). While this system allows ships to be aware and keep track of other ships in their immediate vicinity, coastal states will also be able to receive, plot and log the data by means of base stations along the coast.

Considering the historical AIS contacts of the area under study (see gray lines in Fig. 5), we note that there are some geographical regions where the traffic shows a certain regularity and the main maritime traffic is mostly concentrated there. These are the sea lanes or routes. The proposed KB tracking strategy is aimed to exploit this kind of information to mitigate the problem of the target fragmentation. Similar conditions are present in the case of the ground tracking, in which there are on-road targets following predetermined trajectories and off-road targets moving freely in the region. Analogously, a vessel can follow a route or can move more irregularly (for instance during fishing operations).

AIS historical data, if properly mined and represented, may lead to the statistical description of the area of interest in terms of expected trajectory patterns and motion that constitutes the knowledge inferred from the history of the traffic over the area

¹The AIS is required for all the ships exceeding 300 gross tonnage and engaged on international voyages, for all cargo ships of 500 gross tonnage, not engaged on international voyages, and all passenger ships. On average, a gross weight of 300 tons corresponds to a length of about 25 m.

of interest. The characterization of the routes is out of the scope of the present work. The literature on the subject is abundant, and in the interests of brevity we cite only [27]–[30].

The KB tracking procedure, adopted here, integrates the information about the ship traffic represented as a set of geographical sea lanes, we associate at each of them a specific dynamic model, as formalized in the following sections.

B. On/Off-sea lane Dynamic Models

The target dynamic is defined in Cartesian coordinates [10]

$$\mathbf{x}_k = \mathbf{f}_k(\mathbf{x}_{k-1}, \mathbf{w}_k), \quad (1)$$

where $\mathbf{f}_k(\cdot)$ is a non-linear function at time k , \mathbf{x}_k is the target motion state vector and \mathbf{w}_k is the so-called process noise.

Given the common motion behavior of large vessels, the constant velocity model is adopted [10]

$$\mathbf{x}_k = \mathbf{F}_k \mathbf{x}_{k-1} + \mathbf{\Gamma}_k \mathbf{v}_k, \quad (2)$$

where $\mathbf{x}_k = [x_k, v_{x_k}, y_k, v_{y_k}]^T$, x_k, y_k are the position components along x, y directions, v_{x_k}, v_{y_k} are the corresponding velocity components

$$\mathbf{F}_k = \begin{bmatrix} 1 & T_k & 0 & 0 \\ 0 & 1 & 0 & 0 \\ 0 & 0 & 1 & T_k \\ 0 & 0 & 0 & 1 \end{bmatrix}, \quad \mathbf{\Gamma}_k = \begin{bmatrix} T_k^2/2 & 0 \\ T_k & 0 \\ 0 & T_k^2/2 \\ 0 & T_k \end{bmatrix},$$

T_k is the current sampling time, \mathbf{v}_k takes into account the target acceleration and the unmodeled dynamics, and is assumed to be Gaussian with zero-mean and covariance matrix \mathbf{Q}_k . According to the motion of the ship (off-sea lane/on-sea lane), we can define two different matrices \mathbf{Q}_k .

We handle the motion along a sea lane with the concept of “directional process noise”, see also [8]. The standard motion models assume that the target can move in any direction and, therefore, use equal process noise variances in both the X and Y directions of the Cartesian system. This means that for off-sea lane targets the motion uncertainties in both directions are equal. For on-sea lane targets, the sea lane constraint means more uncertainty along the sea lane than orthogonal. Thus, the IMM module representing on-sea lane motion consists of process noise components along and orthogonal to the sea lane, rather than in the X and Y directions as in the standard motion model.

In the latter case, the motion model is matched with the direction of the sea lane ψ . From different sea lanes we have different values of ψ and therefore different models. In the off-sea lane target motion model, process noise components along X and Y directions are given by v_x and v_y , respectively. Variances of the noise components in the corresponding directions are given by σ_x^2 and σ_y^2 . Similarly, for the on-sea lane target motion model, the process noise component and its variance along the direction of the sea lane are given by v_a and σ_a^2 , respectively. The corresponding values orthogonal to the sea lane are given by v_o and σ_o^2 . Due to the higher motion uncertainty along the sea lane than orthogonal, we assume $\sigma_a \gg \sigma_o$. This is a key element that is in contrast with the typical assumption $\sigma_x = \sigma_y$ used for the off-sea lane motion model, see, *e.g.*, [6].

Starting from Eq. (2), we can have two categories of models by choosing different covariances of the Gaussian process noise at time k , *i.e.* Q_k . The first one is:

$$Q_k = \begin{pmatrix} \sigma_x^2 & 0 \\ 0 & \sigma_y^2 \end{pmatrix}, \quad (3)$$

with $\sigma_x^2 = \sigma_y^2$ used for the off-sea lane targets.

In the second case, since the state estimation is carried out in the X - Y coordinate system, the variances of the process noise components along and orthogonal to the sea lane need to be converted into the covariance matrix. Thus, we have [8]

$$Q_k = \begin{pmatrix} -\cos \psi & \sin \psi \\ \sin \psi & \cos \psi \end{pmatrix} \begin{pmatrix} \sigma_o^2 & 0 \\ 0 & \sigma_a^2 \end{pmatrix} \begin{pmatrix} -\cos \psi & \sin \psi \\ \sin \psi & \cos \psi \end{pmatrix}, \quad (4)$$

where ψ is the direction of the considered sea lane.

In Sec. III-D we establish the method selecting the proper motion dynamic based on the on-line data gathered from the radar.

C. Observation Model

Assuming a radar located at the origin of the spherical coordinates, the target-originated measurement equation can be expressed as

$$\mathbf{z}_k = \mathbf{h}(\mathbf{x}_k) + \mathbf{n}_k, \quad (5)$$

the radar measures the target range, bearing (azimuth), and range rate, then Eq. (5) can be recast as follows

$$\begin{aligned}
\mathbf{z}_k &= [z_k^r, z_k^b, z_k^{\dot{r}}]^T, \\
\mathbf{n}_k &= [n_k^r, n_k^b, n_k^{\dot{r}}]^T, \\
\mathbf{h}(\mathbf{x}_k) &= [h_r(\mathbf{x}_k), h_b(\mathbf{x}_k), h_{\dot{r}}(\mathbf{x}_k)], \\
h_r(\mathbf{x}_k) &= \sqrt{x_k^2 + y_k^2}, \\
h_b(\mathbf{x}_k) &= \arctan\left(\frac{y_k}{x_k}\right), \\
h_{\dot{r}}(\mathbf{x}_k) &= \frac{x_k v_{x_k} + y_k v_{y_k}}{\sqrt{x_k^2 + y_k^2}},
\end{aligned} \tag{6}$$

where $z_k^r, z_k^b, z_k^{\dot{r}}$ are radar measurements of the target range, bearing, and range rate. The measurement noise vector \mathbf{n}_k is assumed to be Gaussian with zero-mean and covariance matrix \mathbf{R}_k given by

$$\mathbf{R}_k = \begin{bmatrix} \sigma_r^2 & 0 & \rho\sigma_r\sigma_{\dot{r}} \\ 0 & \sigma_b^2 & 0 \\ \rho\sigma_r\sigma_{\dot{r}} & 0 & \sigma_{\dot{r}}^2 \end{bmatrix}.$$

Note that in literature [10], [31] $n_k^r, n_k^b, n_k^{\dot{r}}$ are all assumed to be statistically independent, except for n_k^r and $n_k^{\dot{r}}$, which are correlated with a correlation coefficient ρ estimated as in [32].

D. VS-IMM Estimator

In this section we focus on the VS-IMM Estimator in the case of a generic r^{th} target. Let us indicate with \mathcal{S}_k^r the set of dynamic modes for the target r at time k . The possible modes are given by all the on/off-sea lane dynamics described in Sec. III-B. Clearly, we have as on-sea lane modes all the identified maritime routes.

It is assumed that the true target state evolves according to one of the modes in \mathcal{S}_k^r . Let us indicate with $\mu_k^{j_r}$ the probability that mode $j_r \in \mathcal{S}_k^r$ is used by the target r during the above scan, and with $p_{s_r, j_r}[\mathcal{S}_{k-1}^r, \mathcal{S}_k^r]$ the transition probability from mode s_r at time $k-1$ to mode j_r at time k , which depends on the sets \mathcal{S}_{k-1}^r and \mathcal{S}_k^r . The mode-conditioned state estimate and the associated covariance of the filter module $j_r \in \mathcal{S}_k^r$ are denoted by $\hat{\mathbf{x}}_k^{j_r}$ and $\mathbf{P}_k^{j_r}$, respectively. Starting from these definitions, the steps of the VS-IMM estimator are the following.

1) *Step 1 (Mode Set Update)*: Based on the state estimate at time $k - 1$ and the a priori information about the geographical region exploited by the historical AIS data, the mode set of the IMM estimator is updated

$$\mathcal{S}_k^r = \{j_r \in \mathcal{S}^a | \mathcal{S}_{k-1}^r, \mathcal{R}, \mathbf{Z}_1^{k-1}\} = \{j_r \in \mathcal{S}^a | \mathcal{S}_{k-1}^r, \mathcal{R}, \{\hat{\mathbf{x}}_{k-1}^{s_r}, \mathbf{P}_{k-1}^{s_r}, s_r \in \mathcal{S}_{k-1}^r\}\}, \quad (7)$$

where \mathbf{Z}_m^n is the cumulative set of measurements from time m up to time n including target-originated measurements (5) and false alarms, \mathcal{S}^a is the set of all the possible dependent motion modes and \mathcal{R} is the map of sea lanes obtained by the historical AIS data. In Sec. III-E1 we will defined how to adaptively select the IMM filter modules.

2) *Step 2 (Mode Interaction/Mixing)*: The mode-conditioned state estimates of the filter modules from the previous iteration (time $k - 1$) are used to obtain the initial condition for the mode-matched filters at time k . The same is carried out for the covariance matrix.

The initial estimate for filter modules $j_r \in \mathcal{S}_k^r$ is evaluated using

$$\hat{\mathbf{x}}_{\mathbf{0}k-1}^{j_r} = \sum_{s_r \in \mathcal{S}_{k-1}^r} \hat{\mathbf{x}}_{k-1}^{s_r} \mu_{k-1}^{s_r | j_r}, \quad (8)$$

where

$$\mu_{k-1}^{s_r | j_r} = \frac{p_{s_r, j_r}[\mathcal{S}_{k-1}^r, \mathcal{S}_k^r] \mu_{k-1}^{s_r}}{\sum_{l_r \in \mathcal{S}_{k-1}^r} p_{l_r, j_r}[\mathcal{S}_{k-1}^r, \mathcal{S}_k^r] \mu_{k-1}^{l_r}}, \quad s_r \in \mathcal{S}_{k-1}^r, j_r \in \mathcal{S}_k^r \quad (9)$$

are the mixing probabilities. The covariance matrix associated with the above initial condition is given by:

$$\mathbf{P}_{\mathbf{0}k-1}^{j_r} = \sum_{s_r \in \mathcal{S}_{k-1}^r} \mu_{k-1}^{s_r | j_r} \cdot [\mathbf{P}_{k-1}^{s_r} + (\hat{\mathbf{x}}_{k-1}^{s_r} - \hat{\mathbf{x}}_{\mathbf{0}k-1}^{j_r}) \cdot (\hat{\mathbf{x}}_{k-1}^{s_r} - \hat{\mathbf{x}}_{\mathbf{0}k-1}^{j_r})^T], \quad j_r \in \mathcal{S}_k^r. \quad (10)$$

3) *Step 3 (Mode-Conditioned Filtering)*: Using the initial conditions evaluated in *Step 2*, that is, $\hat{\mathbf{x}}_{\mathbf{0}k-1}^{j_r}$ and $\mathbf{P}_{\mathbf{0}k-1}^{j_r}$, $j_r \in \mathcal{S}_k^r$ we can obtain $\hat{\mathbf{x}}_k^{j_r}$ and $\mathbf{P}_k^{j_r}$, $j_r \in \mathcal{S}_k^r$, respectively, see Sec. III-F. In addition to the estimate and the covariance, the likelihood of each filter module $\Lambda_k^{j_r}$, $j_r \in \mathcal{S}_k^r$, which quantifies the goodness of the corresponding motion model, is also evaluated. For more details, in the case of Multiple Model JPDA, see Sec. III-F.

4) *Step 4 (Mode Probability Update)*: Starting from the likelihood, obtained at the previous step, the probability that the mode j_r is in effect at time k , denoted by $\mu_k^{j_r}$, is updated via:

$$\mu_k^{j_r} = \frac{\Lambda_k^{j_r} \sum_{l_r \in \mathcal{S}_{k-1}^r} p_{l_r, j_r}[\mathcal{S}_{k-1}^r, \mathcal{S}_k^r] \mu_{k-1}^{l_r}}{\sum_{s_r \in \mathcal{S}_k^r} \Lambda_k^{s_r} \sum_{l_r \in \mathcal{S}_{k-1}^r} p_{l_r, s_r}[\mathcal{S}_{k-1}^r, \mathcal{S}_k^r] \mu_{k-1}^{l_r}}, \quad j_r \in \mathcal{S}_k^r. \quad (11)$$

5) *Step 5 (State Combination)*: Finally, the mode-conditioned estimates and covariances are combined to find the overall estimate and covariance:

$$\hat{\mathbf{x}}_k = \sum_{j_r \in \mathcal{S}_k^r} \mu_k^{j_r} \hat{\mathbf{x}}_k^{j_r}, \quad (12)$$

$$\mathbf{P}_k = \sum_{j_r \in \mathcal{S}_k^r} \mu_k^{j_r} \cdot [\mathbf{P}_k^{j_r} + (\hat{\mathbf{x}}_k^{j_r} - \hat{\mathbf{x}}_k) \cdot (\hat{\mathbf{x}}_k^{j_r} - \hat{\mathbf{x}}_k)^T]. \quad (13)$$

E. Adaptive Filter Module Selection

1) *Entry/Exit Conditions*: When an off-sea lane target enters the vicinity of a sea lane, it could become an on-sea lane target. Similarly, a target on a sea lane may leave it. Unlike an off-sea lane target, which is free to move in any direction, the motion of an on-sea lane target is highly directional along the sea lane. In view of the highly directional motion of on-sea lane targets, when it is determined that an off-sea lane target is in the vicinity of a sea lane, a new mode, representing motion along that sea lane, is added to the mode set. Similarly, a decision is made as to whether the considered target leaves the vicinity of a sea lane, in the case the related mode is removed.

One of the major issue in adding or deleting modes to handle on-sea lane/off-sea lane motion is deciding when to add or delete, *i.e.*, how to determine that a target enters or leaves the vicinity of a sea lane which allows entry or exit.

Thus, at time k , for each established track r , a decision is made about which sea lanes the target can follow. This is carried out by testing whether the predicted location lies within a certain neighbourhood ellipsoid of any sea lane (for instance, neighbourhood ellipsoids for the real cases can be seen in Fig. 5). A problem of the above decision process is that the target has several modes at time $k - 1$ with their own predicted states and covariances and consequently there is not a unique state/covariance prediction. A possible solution is that if at least one of these predicted states lies inside the ellipsoid then we add the related sea lane mode. At each time interval a sea lane neighbourhood test is carried out for each track against all the sea lanes defined. Modes corresponding to sea lanes not validated are removed from the mode set. Using the above validation strategy, entry into or exit from sea lanes is handled by the estimator.

2) *Obscuration Conditions*: Assume that a target follows a given sea lane and, for some reasons (such as, the first order Bragg scattering or radar synchronization), it is not visible (no detections are associated). Then, some prior information needs to be exploited in order to obtain the target state estimate, its covariance and the filter-calculated likelihood. The UKF state estimate and the VS-IMM equations do not take into account the target visibility, *i.e.*, they assume that the target is always visible. When an active track follows the sea lane mode and there are no associated observations then the estimator is defined as follows.

The filter module corresponding to that sea lane is replaced with a “hidden target” model that modifies the filter estimates and likelihoods accordingly using the information that the target detection probability is zero. The hidden-target model is similar to the “dead-target” model [10] that is commonly used for track termination. The hidden target model accounts for the event that the target has become unobservable. For this model, the state estimate of the target r under the mode of the j^{th} sea lane at time k , *i.e.*, $\hat{\mathbf{x}}_k^{j_r}$ and the associated covariance $\mathbf{P}_k^{j_r}$, are given by:

$$\hat{\mathbf{x}}_k^{j_r} = \hat{\mathbf{x}}_{k|k-1}^{j_r}, \quad (14)$$

$$\mathbf{P}_k^{j_r} = \mathbf{P}_{k|k-1}^{j_r}, \quad (15)$$

where $\hat{\mathbf{x}}_{k|k-1}^{j_r}$ and $\mathbf{P}_{k|k-1}^{j_r}$ are the predicted estimate and its covariance under the mode j of the target r at time k as classically defined in the UKF prediction equations (see [11], [19] for further details).

Since the measurement is not used in the state estimate, a similar modification is required in evaluating the filter-calculated likelihood, which quantifies, in the VS-IMM Estimator, the filter's confidence in the measurement. The following expression is used for the likelihood of the hidden target r under the mode of the j^{th} sea lane at time k :

$$\Lambda_k^{j_r} \stackrel{\text{def}}{=} \frac{1}{V}, \quad (16)$$

where V is the filter gate volume given by

$$V = \gamma^{n_z/2} V_{n_z} |\mathbf{S}_k^{j_r}|^{1/2}, \quad (17)$$

and V_{n_z} is the volume of the unit hypersphere of dimension n_z , n_z is the cardinality of the measurement \mathbf{z} (*i.e.* 3 in this case), γ is the gate size used for the measurement validation (equal to 5) and $\mathbf{S}_k^{j_r}$ is the innovation covariance of the target r under the mode j_r at time k . For radar measurements with range, azimuth and range rate, $V_{n_z} = \frac{4\pi}{3}$ [10]. For the ‘‘hidden target’’ model, which treats the measurement as a spurious one, V^{-1} is the filter-calculated clutter density in its validation gate.

The ‘‘hidden target’’ model is removed from the mode set if one of the following conditions become true: *i*) the target becomes visible again; *ii*) the corresponding sea lane segment is no longer validated.

F. Data Association: The Multiple Model JPDA

The VS-IMM equations, presented in the previous subsections, assume that a measurement is always available to update the estimates of a track. In the case the single received measurement is used to update the single active track. However, in multi-target tracking scenarios in presence of target miss detections and false alarms, it is necessary to decide which one of the received measurements should be used to update a particular track. It is required a data association mechanism (measurement-to-track association). In this section the Multiple Model JPDA algorithm, *e.g.* see [33], is exploited to deal with this issue.

The following notations will be used. Let $\mathbf{Z}_1^k = [\mathbf{Z}_1, \dots, \mathbf{Z}_k]$ be the set of all measurements up to time k where the generic set $\mathbf{Z}_k = [\mathbf{z}_k^1, \dots, \mathbf{z}_k^i, \dots, \mathbf{z}_k^m]$ represents the measurements at time k . Let \mathbf{T}_k the set of targets at time k with cardinality $N_k = |\mathbf{T}_k|$.

We now focus our attention on the time k for a particular target $r \in \mathbf{T}_k$. Assume that for the target r at time k there is a set of allowed modes $\mathcal{S}_k^r \subset \mathcal{M}_n$ where \mathcal{M}_n is the set of all possible n modes. Let $M_k^{j_r}$ denote the event that the mode j_r is in effect at time k for the target r .

First of all, in order to reduce the computation burden of the algorithm a measurement validation, often referred as gating, is performed [10]. Starting from the measurements \mathbf{Z}_k at time k , a subset $\mathbf{Y}_k = [\mathbf{y}_k^1, \dots, \mathbf{y}_k^i, \dots, \mathbf{y}_k^{\bar{m}}]$, $\bar{m} \leq m$, is generated containing only validated measurements, *i.e.* the gating condition [6] is verified for at least one mode of a target. The cumulative set up to time k is indicated as \mathbf{Y}_1^k .

A marginal association event θ_{ir} is said to be effective at time k when the i^{th} validated measurement \mathbf{y}_k^i is associated with target r ($r = 0, \dots, N_k$ where $r = 0$ means that the measurement is caused by clutter). Assuming that there are no unresolved measurements, a joint association event Θ is effective when a set of marginal events $\{\theta_{ir}\}$ holds true simultaneously. That is, $\Theta = \cap_{i=1}^{\bar{m}} \theta_{ir}$ where r is the target index associated to \mathbf{y}_k^i . Define the validation matrix:

$$\Omega = [\omega_{ir}], \quad i = 1, \dots, \bar{m}, \quad r = 0, \dots, N_k, \quad (18)$$

where $\omega_{ir} = 1$ if the measurement i lies in the validation gate of the target r , else it is zero. A joint association event Θ is represented by the event matrix

$$\hat{\Omega}(\Theta) = [\hat{\omega}_{ir}(\Theta)], \quad i = 1, \dots, \bar{m}, \quad r = 0, \dots, N_k, \quad (19)$$

where $\hat{\omega}_{ir} = 1$ if $\theta_{ir} \subset \Theta$ and $\hat{\omega}_{ir} = 0$ otherwise. A feasible association event can have only one source (target or clutter), *i.e.* for each i , $\sum_{r=0}^{N_k} \hat{\omega}_{ir}(\Theta) = 1$, and where at most one measurement can be originated by a target, *i.e.*, $\delta_r(\Theta) \stackrel{\text{def}}{=} \sum_{i=0}^{\bar{m}} \hat{\omega}_{ir}(\Theta) \leq 1$ for $r = 1, \dots, N_k$. The above joint events Θ are mutually exclusive and exhaustive. Define the binary measurement association indicator $\tau_i(\Theta) \stackrel{\text{def}}{=} \sum_{r=1}^{N_k} \hat{\omega}_{ir}(\Theta)$, $i = 1, \dots, \bar{m}$, to indicate whether the validated measurement \mathbf{y}_k^i is associated with a target in event Θ . Further, the number of false (unassociated) measurements in event Θ is $\phi(\Theta) = \sum_{i=1}^{\bar{m}} [1 - \tau_i(\Theta)]$. One can evaluate the likelihood that the target r is in mode j_r at time k as

$$\Lambda_k^{j_r} \stackrel{\text{def}}{=} \sum_{\Theta} p[\mathbf{Y}_k | \Theta, M_k^{j_r}, \mathbf{Y}_1^{k-1}] P\{\Theta\} \quad (20)$$

The first term in Eq. (20) for the law of total probability can be written as [33]

$$\begin{aligned} p[\mathbf{Y}_k | \Theta, M_k^{j_r}, \mathbf{Y}_1^{k-1}] &= \sum_{j_1 \in \mathcal{S}_k^1} \dots \sum_{j_{r-1} \in \mathcal{S}_k^{r-1}} \dots \sum_{j_{r+1} \in \mathcal{S}_k^{r+1}} \dots \sum_{j_{N_k} \in \mathcal{S}_k^{N_k}} \\ & p[\mathbf{Y}_k | \Theta, M_k^{j_1}, \dots, M_k^{j_{r-1}}, M_k^{j_r}, M_k^{j_{r+1}}, \dots, M_k^{j_{N_k}}, \mathbf{Y}_1^{k-1}] \\ & P\{M_k^{j_1}, \dots, M_k^{j_{r-1}}, M_k^{j_{r+1}}, \dots, M_k^{j_{N_k}} | \Theta, M_k^{j_r}, \mathbf{Y}_1^{k-1}\}. \end{aligned} \quad (21)$$

The second term (a prior joint association probabilities) in Eq. (20) turns out to be²

$$P\{\Theta\} = \exp(-\lambda V) \cdot \frac{(\lambda V)^{\phi(\Theta)}}{\bar{m}!} \prod_{s=1}^{N_k} [P_D^{\delta_s(\Theta)} \cdot (1 - P_D)^{1 - \delta_s(\Theta)}] \quad (22)$$

²Note that here we use the parametric model of the clutter density instead of the nonparametric one used in [33].

where P_D is the detection probability (assumed to be the same for all targets), λ is the spatial density of the false measurements and V is the volume of the validation region. We assume that the states of the targets (including the modes) conditioned on the past observations are mutually independent. Then the first term on the right hand side of Eq. (21) can be written as [33]

$$p[\mathbf{Y}_k | \Theta, M_k^{j_1}, \dots, M_k^{j_{r-1}}, M_k^{j_r}, M_k^{j_{r+1}}, \dots, M_k^{j_{N_k}}, \mathbf{Y}_1^{k-1}] \approx \prod_{i=1}^{\bar{m}} p[\mathbf{y}_k^i | \theta_{ir}, M_k^{j_r}, \mathbf{Y}_1^{k-1}], \theta_{ir} \subset \Theta, \quad (23)$$

where the conditional probability density function of the validated measurement \mathbf{y}_k^i given its origin and target mode, is given by

$$p[\mathbf{y}_k^i | \theta_{ir}, M_k^{j_r}, \mathbf{Y}_1^{k-1}] = \begin{cases} \mathcal{N}(\mathbf{y}_k^i; \hat{\mathbf{z}}_k^{j_r}, \mathbf{S}_k^{j_r}), & \text{if } \tau_i(\Theta) = 1, \\ 1/V, & \text{if } \tau_i(\Theta) = 0, \end{cases} \quad (24)$$

where $\mathcal{N}(\mathbf{x}; \mu, \Sigma)$ is the multivariate Gaussian with mean μ and covariance Σ , the terms $\hat{\mathbf{z}}_k^{j_r}$ and $\mathbf{S}_k^{j_r}$ are the measurement prediction and the innovation matrix, respectively, obtained by the target r under the mode j_r using UKF (see [11], [19] for details) because of the non-linearity in the state-to-measurement relationship. The second term on the right hand side of Eq. (21) is given by:

$$P\{M_k^{j_1}, \dots, M_k^{j_{r-1}}, M_k^{j_{r+1}}, \dots, M_k^{j_{N_k}} | \Theta, M_k^{j_r}, \mathbf{Y}_1^{k-1}\} = \prod_{s=1, s \neq r}^{N_k} \mu_k^{j_s} \quad (25)$$

The probability of the joint association event Θ given that mode j_r is effective for the target r from time $k-1$ through k is

$$P\{\Theta | M_k^{j_r}, \mathbf{Y}_1^{k-1}, \mathbf{Y}_k\} = \frac{1}{c} p[\mathbf{Y}_k | \Theta, M_k^{j_r}, \mathbf{Y}_1^{k-1}] P\{\Theta\}, \quad (26)$$

where the first term can be calculated from Eq. (21) and Eqs. (23) - (25), the second term from Eq. (22), and c is a normalization constant. Then the probability of the marginal association event is given by:

$$\beta_k^{i, j_r} \stackrel{def}{=} P\{\theta_{ir} | M_k^{j_r}, \mathbf{Y}_1^{k-1}, \mathbf{Y}_k\} = \sum_{\Theta: \theta_{ir} \subset \Theta} P\{\Theta | M_k^{j_r}, \mathbf{Y}_1^{k-1}, \mathbf{Y}_k\}. \quad (27)$$

The following updates are done for each target r . Calculate $\Lambda_k^{j_r}$ via Eqs. (20) - (25). Calculate β_k^{i, j_r} via Eqs. (21) - (27). Define the target and mode-conditioned innovations for each validated measurement $i = 1, \dots, \bar{m}$ as

$$\nu_k^{i, j_r} \stackrel{def}{=} \mathbf{y}_k^i - \hat{\mathbf{z}}_k^{j_r}, \quad (28)$$

Using the predicted state estimation $\hat{\mathbf{x}}_{k|k-1}^{j_r}$ and its covariance $\mathbf{P}_{k|k-1}^{j_r}$ obtained by the Unscented Kalman Filter [11], [19] starting from the estimates calculated in the Interaction/Mixing step Sec. III-D by means of the models in Sec. III-B, one computes the partial update $\hat{\mathbf{x}}_k^{j_r}$ and its covariance $\mathbf{P}_k^{j_r}$ according to the standard PDAF [10]. Defining the target-dependent combined mode-conditioned innovation:

$$\nu_k^{j_r} = \sum_{i=1}^{\bar{m}} \beta_k^{i, j_r} \nu_k^{i, j_r} \quad (29)$$

we have:

$$\hat{\mathbf{x}}_k^{j_r} = \hat{\mathbf{x}}_{k|k-1}^{j_r} + \mathbf{W}_k^{j_r} \nu_k^{j_r} \quad (30)$$

$$\mathbf{P}_k^{j_r} = \mathbf{P}_{k|k-1}^{j_r} - \left(\sum_{i=1}^{\bar{m}} \beta_k^{i,j_r} \right) \mathbf{W}_k^{j_r} \mathbf{S}_k^{j_r} (\mathbf{W}_k^{j_r})^T + \mathbf{W}_k^{j_r} \left[\sum_{i=1}^{\bar{m}} \beta_k^{i,j_r} \nu_k^{i,j_r} (\nu_k^{i,j_r})^T - \nu_k^{j_r} (\nu_k^{j_r})^T \right] (\mathbf{W}_k^{j_r})^T \quad (31)$$

where $\mathbf{W}_k^{j_r}$ is the Kalman Gain [11], [19].

After calculating $\hat{\mathbf{x}}_k^{j_r}$, $\mathbf{P}_k^{j_r}$ and $\Lambda_k^{j_r}$ for each $j_r \in \mathcal{S}_k^r$, one can use them in Step 4 and Step 5 of the VS-IMM Estimator (described in Sec. III-D) for the r^{th} target. In Algorithm 1 a summary of the VS-IMM JPDA algorithm for the r^{th} target at time k is shown.

Algorithm 1 VS-IMM JPDA for a target r at time k

$[\{\hat{\mathbf{x}}_k^{j_r}, \mathbf{P}_k^{j_r}, \mu_k^{j_r}, j_r \in \mathcal{S}_k^r\}, \hat{\mathbf{x}}_k, \mathbf{P}_k] = \text{VS-IMM JPDA}[\{\hat{\mathbf{x}}_{k-1}^{s_r}, \mathbf{P}_{k-1}^{s_r}, \mu_{k-1}^{s_r}, s_r \in \mathcal{S}_{k-1}^r\}, \mathbf{Y}_k]$

- Define a mode set \mathcal{S}_k^r as in Sec. III-D1.

if there is no validated measurement for r in \mathbf{Y}_k **and** r follows the on-sea lane mode j_r **then**

- Add the “hidden target” model defined by Eqs. (14)-(16) in \mathcal{S}_k^r .

- Remove the mode j_r in \mathcal{S}_k^r .

end if

for $j_r \in \mathcal{S}_k^r$ **do**

- Calculate $\hat{\mathbf{x}}_{0k}^{j_r}$ and $\mathbf{P}_{0k}^{j_r}$ starting from $\{\hat{\mathbf{x}}_{k-1}^{s_r}, \mathbf{P}_{k-1}^{s_r}, \mu_{k-1}^{s_r}, s_r \in \mathcal{S}_{k-1}^r\}$ as in Eqs. (8)-(10).

- Calculate the predicted state estimation $\hat{\mathbf{x}}_{k|k-1}^{j_r}$ and its covariance $\mathbf{P}_{k|k-1}^{j_r}$ starting from $\hat{\mathbf{x}}_{0k}^{j_r}$ and $\mathbf{P}_{0k}^{j_r}$ using UKF [11], [19].

- Calculate $\Lambda_k^{j_r}$, $\hat{\mathbf{x}}_k^{j_r}$ and $\mathbf{P}_k^{j_r}$ starting from $\hat{\mathbf{x}}_{k|k-1}^{j_r}$, $\mathbf{P}_{k|k-1}^{j_r}$ and \mathbf{Y}_k using Eq. (20), Eqs. (30)-(31), respectively.

- Calculate $\mu_k^{j_r}$ using Eq. (11).

end for

- Combine $\{\hat{\mathbf{x}}_k^{j_r}, \mathbf{P}_k^{j_r}, \mu_k^{j_r}, j_r \in \mathcal{S}_k^r\}$ to obtain $\hat{\mathbf{x}}_k$ and \mathbf{P}_k for the target r by Eqs. (12)-(13).

G. Track Management

1) *Track Formation*: The M-of-N rule is used for the track initiation, see details in [10]. If the requirement is satisfied, then the measurement sequence is accepted as a valid track.

The following logic that assumes target position measurements is considered

- Every unassociated measurement is an *initiator*, i.e. it yields a *tentative track*.

- At the sampling time following the detection of an initiator, a gate is set up based on the i) assumed maximum (minimum) target dynamic, ii) the measurement noise intensities, *i.e.* if there is a target that gave rise to the initiator, the possible measurement originated from it in this second scan will fall in the gate with high probability. Following a detection, this track becomes a *preliminary track*. If there is no detection, this tentative track is dropped. Since a preliminary track has two measurements, the UKF can be initialized and used to set up a gate for the next sampling time.
- Starting from the third scan a logic of M detections out of N scans is used for the subsequent gates.
- If at the end (scan $N + 2$) the logic requirement is satisfied, the track becomes a *confirmed track*. Otherwise it is dropped.
- A confirmed track is said *on-sea lane confirmed track* if the target that is generating the track follows the same on-sea lane mode for a period time (*i.e.* it has as main mode an on-sea lane one at least for a certain number of scans W) otherwise it is defined *off-sea lane confirmed track*.

2) *Track Termination*: An on-sea lane confirmed track is terminated if one of the following event occurs:

- The likelihood in Eq. (16) goes down a given threshold τ ;
- The counter that takes into account the number of consecutive scans in which the target is not visible exceeds a given value NNT_{max} ;
- The target's track uncertainty (state covariance matrix) has grown beyond a certain threshold;
- The target has reached an unfeasible maximum velocity v_{max} .

An off-sea lane confirmed track is terminated if one of the following event occurs:

- No detection has been validated for the past M^* out of N^* most recent sampling times;
- The target's track uncertainty (state covariance matrix) has grown beyond a certain threshold;
- The target has reached an unfeasible maximum velocity v_{max} .

IV. EXPERIMENTAL RESULTS

In this section a comparison between the proposed VS-IMM JPDA and the standard JPDA is provided by using both simulated and real data of HFSW radar systems. As already proposed in [6], we use as ground truth for tracking assessment the AIS static/kinematic reports. AIS ship reports are checked in order to remove possible outliers, missing position reports and unreliable data, then, the following key assumptions are made:

- Ships carrying an AIS-transponder are the only ones present in the region of interest (in some cases this could be not true, indeed, reliable tracks, not corresponding to any AIS report, are observed);
- The AIS messages exchanged by ships are reliable and not corrupted by any sort of errors.

This section is organized as follows. The association procedure between the tracks provided by the tracking algorithms and the ground-truth based on AIS contacts is presented in Sec. IV-A. Performance metrics are introduced in Sec. IV-B. Finally, experimental results are presented and discussed in Secs. IV-D and IV-E.

A. Association Procedure

In this section we report the association procedure between radar and AIS contacts, already proposed in [6]. Consider that the time intervals between the AIS reports and the radar timestamps are not aligned, then we have to interpolate the kinematic AIS reports in the HFSW radar timestamps. We define $\bar{\mathcal{X}}_k$ as the set of the AIS tracks at time k , with $\bar{\mathbf{x}}_k = [\bar{x}_k, \bar{v}_{x_k}, \bar{y}_k, \bar{v}_{y_k}]^T \in \bar{\mathcal{X}}_k$, where \bar{x}_k, \bar{y}_k are the positions in the Cartesian coordinates and $\bar{v}_{x_k}, \bar{v}_{y_k}$ are the corresponding velocities. In order to cope with possible unwanted artefacts after this pre-processing phase, we added a flag index that allows us to decide whether the current transmission is reliable or not. Longitude/latitude and Course-Over-Ground (COG)/ Speed-Over-Ground (SOG) information are converted to obtain the current Cartesian vector.

The set of tracks at time k estimated by the KB tracking algorithm is indicated by $\hat{\mathcal{X}}_k$ and a single contact is defined as:

$$\hat{\mathbf{x}}_k = [\hat{x}_k, \hat{v}_{x_k}, \hat{y}_k, \hat{v}_{y_k}]^T, \quad (32)$$

where \hat{x}_k, \hat{y}_k are the positions in the Cartesian coordinates of a generic target at time k and $\hat{v}_{x_k}, \hat{v}_{y_k}$ are the relative velocities.

Let us start describing the association procedure. To each AIS contact $\bar{\mathbf{x}}_k^c$ at time k (with $c = 1, \dots, C_k$) belonging to $\bar{\mathcal{X}}_k$, a single WERA track contact $\hat{\mathbf{x}}_k^n$ (with $n = 1, \dots, N_k$) belonging to $\hat{\mathcal{X}}_k$, can be associated to it.

The association is carried out by searching the nearest among all the radar tracks falling the performance validation region centred on the AIS contact:

$$(\hat{\mathbf{x}}_k^n \rightarrow \bar{\mathbf{x}}_k^c) : d(\hat{\mathbf{x}}_k^n, \bar{\mathbf{x}}_k^c) = \min_{t,j} \{d(\hat{\mathbf{x}}_k^t, \bar{\mathbf{x}}_k^j)\}, \quad (33)$$

where $t = 1, \dots, N_k$, $j = 1, \dots, C_k$, and $d(\cdot, \cdot)$ is a distance metric. If the current $\hat{\mathbf{x}}_k^n$ has a validated track contact $\bar{\mathbf{x}}_k^c$, we define this occurrence as a correct detection and we delete these points from the association procedure, otherwise it is considered a false alarm.

B. Performance Metrics

The performance metrics, already introduced in [6], are briefly described in this section.

- Normalized Time-on-Target (*ToT*): It is defined as the ratio between the length of an active track (correctly associated to the AIS) and the AIS track length. Thus, we have:

$$ToT = \frac{1}{N} \sum_{n=1}^N \frac{\hat{l}_n}{l_n}, \quad (34)$$

where N represents the number of ships in the area under study, l_n and \hat{l}_n are the AIS and radar track lengths, respectively, for the n^{th} ship. The ideal value of the ToT index is 100%, *i.e.*, when $\hat{l}_n = l_n$ for all the tracks in the scenario under test.

- **False Alarm Rate (FAR):** It is defined as the number of false track contacts, normalized with the recording interval and the area of the surveyed region. A false alarm is defined as a contact that does not belong to anyone AIS report. The FAR can be evaluated as following:

$$FAR = \frac{N_{fa}}{A \cdot \Delta T}, \quad (35)$$

where N_{fa} is the number of false alarms, A is the area of the surveyed region (measured in $[\text{m}^2]$) and ΔT is the whole time of the record (measured in $[\text{s}]$). The ideal value of the FAR is 0 (no false alarm).

- **Number of radar tracks N^{TF} associated with a single target:** It is an index that measures the Track Fragmentation (TF). An ideal system would have $N^{TF} = 1$, *i.e.* the radar system is able to follow the whole track without losing it. We typically obtain values of N^{TF} larger than 1.
- **Root Mean Square Error (RMSE):** The error committed by the tracking algorithm has been evaluated. Given the true and the estimated state vectors at time k denoted by $\bar{\mathbf{x}}_k$ and $\hat{\mathbf{x}}_k$, respectively, we can define the RMSE in position and velocity as:

$$\epsilon_k^{pos} = \sqrt{(\hat{x}_k - \bar{x}_k)^2 + (\hat{y}_k - \bar{y}_k)^2}, \quad (36)$$

$$\epsilon_k^{vel} = \sqrt{(\hat{v}_{x_k} - \bar{v}_{x_k})^2 + (\hat{v}_{y_k} - \bar{v}_{y_k})^2}. \quad (37)$$

The relative overall indexes are obtained by averaging ϵ_k^{pos} and ϵ_k^{vel} along the timestamps. These averaged quantities will be indicated with the symbols ϵ^{pos} and ϵ^{vel} , respectively. The ideal values are 0 for both the indexes.

C. Parameter Settings

Some parameters of the algorithms should be properly set in order to obtain acceptable performances. This section is devoted to summarize the selection of these parameters. We can divide them in the following groups:

- **IMM** - The main parameters are related to the transition probabilities among modes in the VS-IMM estimator. In particular, the probability to switch from the off-sea lane to an on-sea lane mode and vice versa is 0.05;
- **Model** - For the dynamic models, the sampling period T_k is about 16.64/33.28 [s]. The standard deviation process noise parameters for the off-sea lane mode are $\sigma_x = \sigma_y = 0.01$ $[\text{m/s}^2]$ while for an on-sea lane mode are $\sigma_o = 0.001$ $[\text{m/s}^2]$ for the component in the sea lane orthogonal direction and $\sigma_a = 0.01$ $[\text{m/s}^2]$ for the component in the along sea lane

direction. The process noises related to the observation model are the same for all the modes. The standard deviation in range (σ_r) is 150 [m], in azimuth (σ_b) is 1.5° and in range rate ($\sigma_{\dot{r}}$) is 0.1 [m/s];

- *Hidden* - The likelihood threshold τ is set to 0.001, the maximum number of scans for which the target can be unobservable NNT_{max} is set to 25. In order to add the “hidden target” model, the number of scans W in which an on-sea lane mode must be the most likely is set to 5;
- *Logic* - The maximum target velocity v_{max} is set to 20 [m/s]. Furthermore, M is chosen to be equal to 5 while N is 6. Furthermore, we choose $M^* = N^*$ in the off-sea lane track termination logic. N^* will be specified for each test case;
- *Detection* - The detection probability P_D is set to 0.35 and the clutter density λ is 10^{-9} [m $^{-2}$].

D. Simulated Results

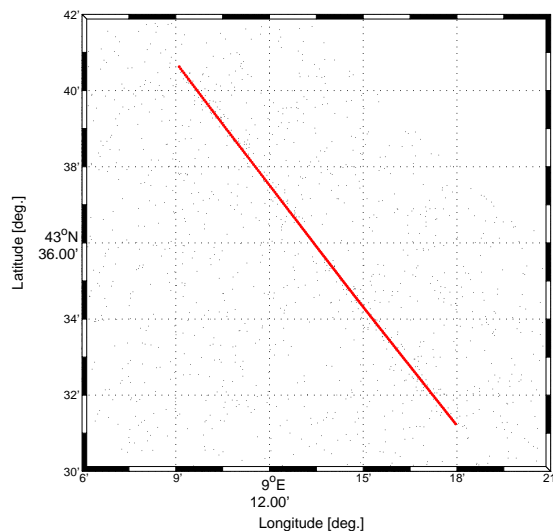


Fig. 2. Simulated scenario: True target contacts of an on-sea lane ship (red), HFSW radar observations (black).

We start presenting simulated radar scenarios. Fig. 2 shows an example of a simulated case with a high clutter environment (the clutter density is about $8 \cdot 10^{-5}$ [m $^{-2}$]). We show the true target track (red) and the simulated HFSW radar observations (black dots). The ship is following a sea lane reported in Fig. 5.

The first analysis is related to the behaviour of the VS-IMM JPDA and the standard JPDA varying the parameter N^* . The results are obtained by averaging 10^3 Monte Carlo (MC) trials. Half of the simulated target trajectories follows the sea lane and are generated accordingly to the directional noise dynamic model described in Sec. III-B. The others do not follow the sea lane and are generated accordingly to the off-sea lane dynamic model, see Sec. III-B. Then, the radar plot is generated in a uniform cluttered environment with a detection probability $P_D = 0.6$. We report the relationship between the ToT and FAR in Fig. 3 for the VS-IMM JPDA and the standard JPDA. It is worthwhile to note that when the parameter N^* grows,

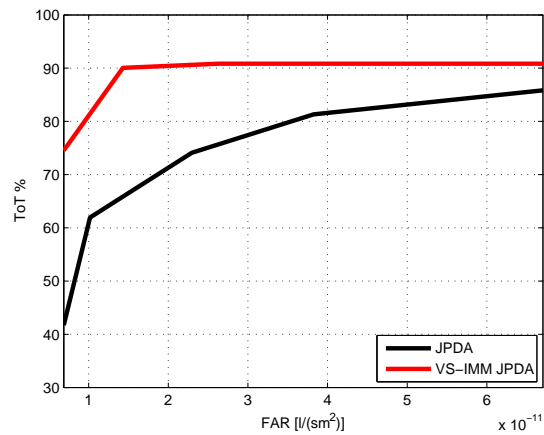


Fig. 3. ToT Vs. FAR varying N^* using a number of MC runs 10^3 .

TABLE I

MEANS AND STANDARD DEVIATIONS OF ϵ^{pos} AND ϵ^{vel} USING A NUMBER OF MC RUNS 10^3 .

	ϵ^{pos} [m]		ϵ^{vel} [m/s]	
	VS-IMM JPDA	JPDA	VS-IMM JPDA	JPDA
mean	379.1	438.2	0.96	1.05
st. dev.	331.7	446.1	0.45	0.58

the FAR and the ToT increase. We have that the VS-IMM outperforms the standard JPDA in terms of ToT/FAR . In other words, for each value of the FAR , we obtain that the ToT of the VS-IMM is higher than the one of the standard JPDA. Furthermore, we point out that in the region where the FAR is small, that represents most important region from an operative point of view, the performance gap between the two approaches is larger.

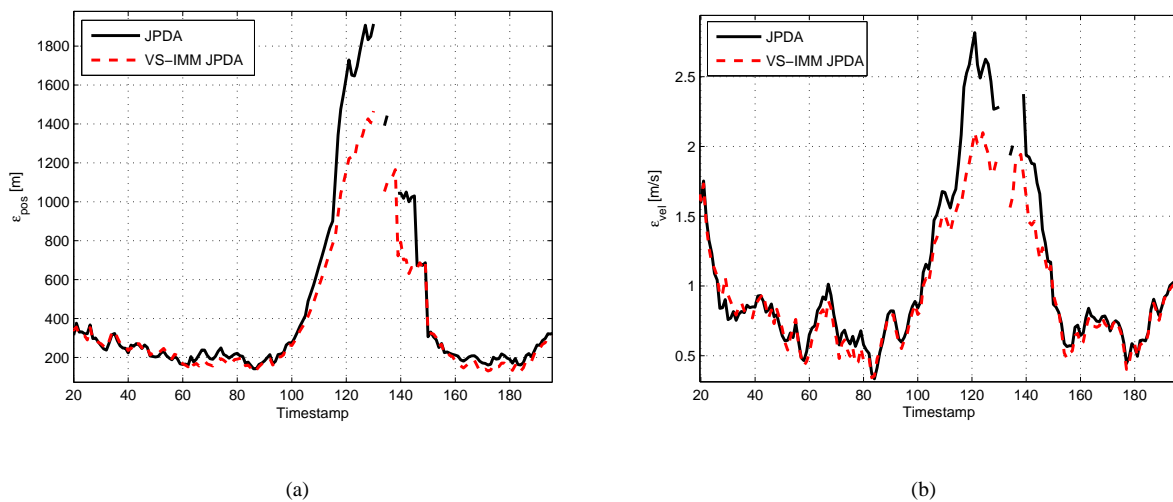


Fig. 4. Average value of (a) ϵ^{pos} and (b) ϵ^{vel} using a number of MC runs 10^3 .

In Figs. 4(a) and 4(b), averaged errors over MC trials ϵ^{pos} and ϵ^{vel} are shown, respectively. In addition with respect to the

previous scenario a fragmentation of the track is simulated (no target-originated detections) between timestamps 100 and 120. A better accuracy of the VS-IMM is exhibited, see also Tab. I where the mean and the standard deviation of the two algorithms on the whole scenario is reported. The gain in terms of performance is sensible in the regions where the target-originated measurements are missed. This is a key element of the proposed KB-tracking methodology: The sea lane knowledge can properly guide the algorithm when no target-originated observations are available.

E. Real Data Performance Assessment

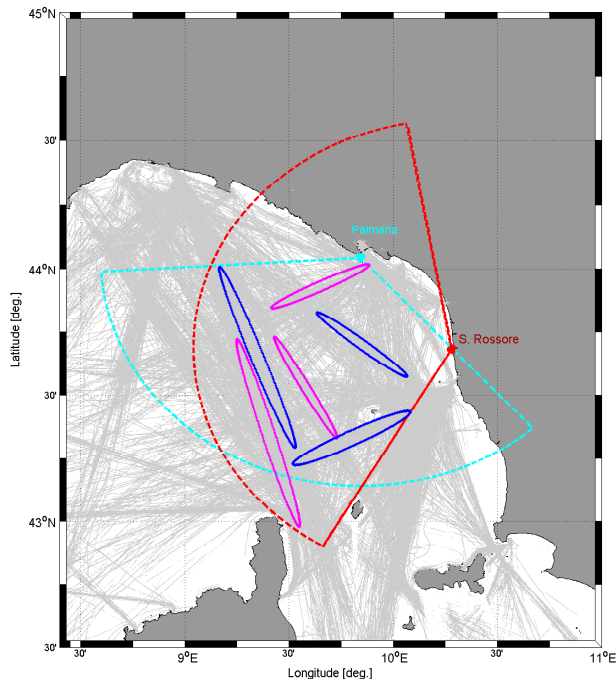


Fig. 5. Real case scenario: In red and cyan the S. Rossore and Palmaria radar fields of view. Magenta ellipsoids indicate the selected areas for the S. Rossore dataset, while, in blue the ones for the Palmaria dataset. Gray lines represent the historical AIS trajectories.

The proposed KB-tracking has been tested on whole dataset provided by the NURC BP09 experiment starting from May 7, 2009 to June 4, 2009. Data from the Palmaria and S. Rossore WERA radar systems (named *Palmaria* and *S. Rossore* datasets) have been separately processed using the *CFAR* algorithm developed at the University of Hamburg. The detections are then provided to the KB-tracking and to the standard JPDA [6].

Fig. 5 depicts the selected areas for the comparison between the VS-IMM and the standard JPDA.

In Fig. 6 an example of the two approaches under test is reported. Tracks generated from both the JPDA and VS-IMM JPDA are depicted in black, while the tracks generated only by the VS-IMM JPDA are depicted in red. No track is generated

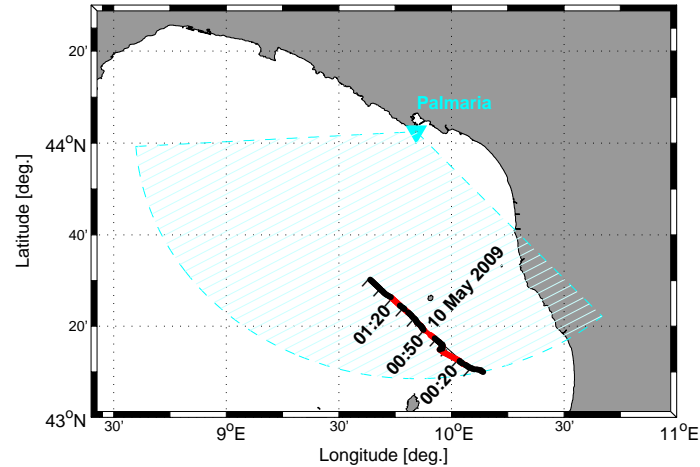


Fig. 6. Graphical representation of the VS-IMM JPDA fragmentation reduction with respect to JPDA using the same track management parameters. Tracks generated from both the JPDA and VS-IMM JPDA are depicted in black, while the tracks generated only by the VS-IMM JPDA are depicted in red.

only by the standard JPDA. The results are obtained by using the parameter setting detailed in Sec. IV-C with $N^* = 5$. It is worthwhile to remark that thanks to the correct identification of the on-sea lane target dynamic, the KB-tracking is able to visibly reduce the N^{TF} and increase the ToT by properly propagating the track when no target-originated observations are received.

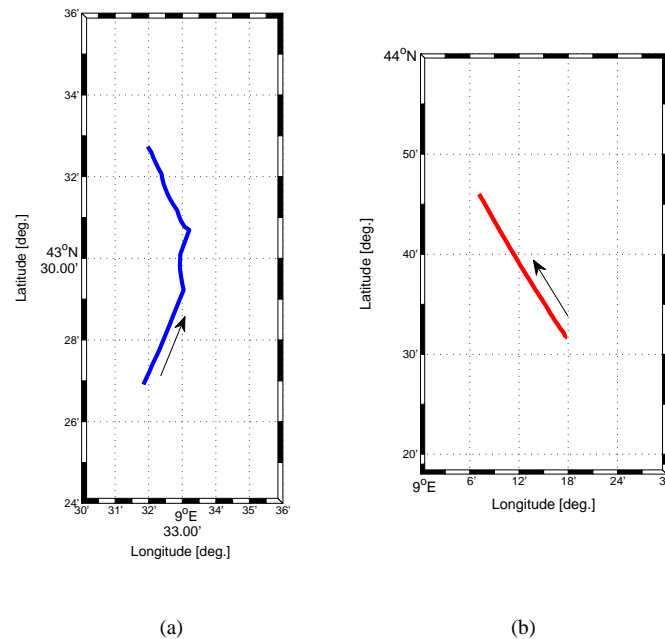


Fig. 7. (a) Off-sea lane Italian cruise (MMSI = 247817000) and (b) on-sea lane Norwegian cargo (MMSI = 258981000) tracks on May 10, 2009. The arrows indicate the directions followed by the vessels.

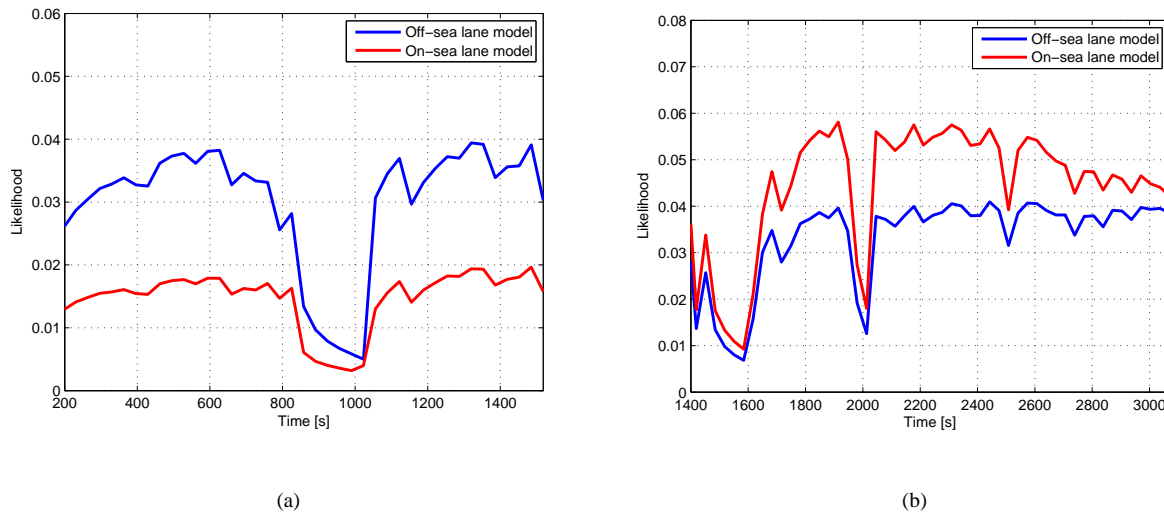


Fig. 8. (a) Off-sea lane and (b) on-sea lane target likelihoods.

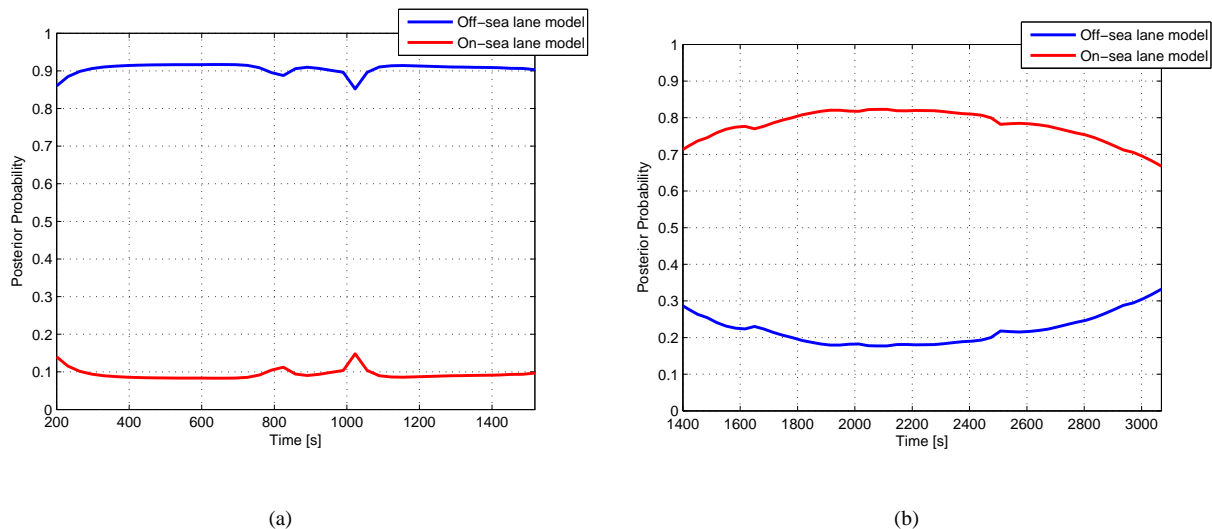


Fig. 9. (a) Off-sea lane and (b) on-sea lane target posterior probabilities.

The capability of the KB-tracking methodology to properly detect on-sea and off-sea lane targets is corroborated presenting two different real cases. The first one shows an off-sea lane Italian cruise, specifically the vessel is manoeuvring to join the sea lane later on. The second case is related to the behaviour of an on-sea lane Norwegian cargo, see Fig. 7. The exploited dynamic models are: The constant velocity with equal standard deviations, which characterizes off-sea lane target dynamics, and the directional noise model which takes into account the information related to the on-sea lane targets. Likelihoods estimated by Eq. (20) and the related posterior probability values, calculated as in Sec. III-D4, are reported in Figs. 8 and 9, respectively. We observe that the estimated likelihoods (which drive the process to have higher posterior probabilities) are coherent with the nature of the true target motions. The system is able to recognize the ship motion and to correctly adopt the model promoting a greater weight. Furthermore, because of the difficulty of predicting the correct target state when this is quickly manoeuvring,

lower values of likelihoods can be observed, for instance see Fig. 8(a) between 800 [s] and 1000 [s].

Before starting the quantitative analysis, we discuss and analyse a further problem. Only some of the target trajectories, which intersect the ellipsoids in Fig. 5, follow the sea lane dynamic models. Now, given the huge amount of data, an automatic procedure, able to properly split the on-sea and off-sea lane ground-truth trajectories, needs to be adopted. Thus, a linear regression applied on each AIS target that crosses the ellipsoids is performed. The R^2 index, provided by the regression, is computed in order to determinate the linearity of the whole sea lane. If this index is larger than a certain threshold (fixed to 0.8), the angular coefficient is computed and compared with the one characterizing the sea lane model to determine the nature of each AIS track.

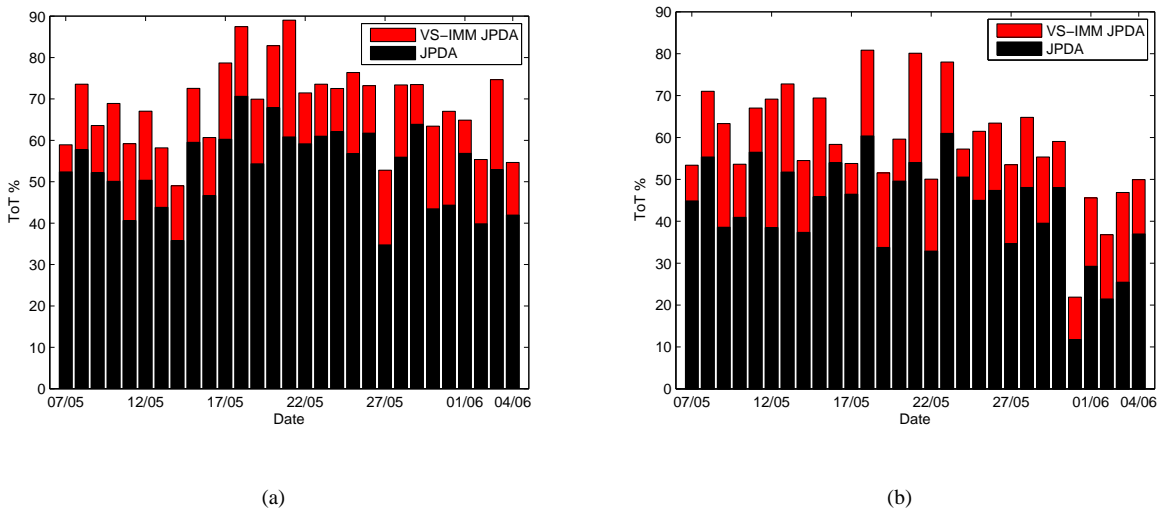


Fig. 10. Daily bar diagram for the ToT evaluated on the (a) Palmaria and (b) S. Rossore datasets. In this case, N^* is equal to 5.

The first quantitative analysis is performed to show the improvements in terms of Time-on-Target (ToT). In Fig. 10, the daily ToT index is reported and obtained by averaging the data of all the on-sea lane targets on each day. The advantage of using the VS-IMM JPDA is clear: We have larger ToT for all the days on both the datasets. Generally speaking, the lower the probability to detect a target is, the greater is the improvement in terms of ToT . Thus, the improvement in terms of performance is more evident when N^* decreases (see Tab. II). Another remark is related to the differences between the Palmaria and S. Rossore datasets. The ToT exhibited by S. Rossore is generally lower than the one on the Palmaria dataset (see, again, Tab. II), as already discussed in [6].

The previous analysis lacks the contribute of the FAR . It is possible that when the FAR increases the ToT increases as well. In order to have a fair comparison, we compare the ToT for both the approaches at fixed FAR values. This curve is obtained by varying the parameter N^* .

In Fig. 11, four scatter plots, which represent the relation between the ToT and FAR indexes varying N^* , are shown.

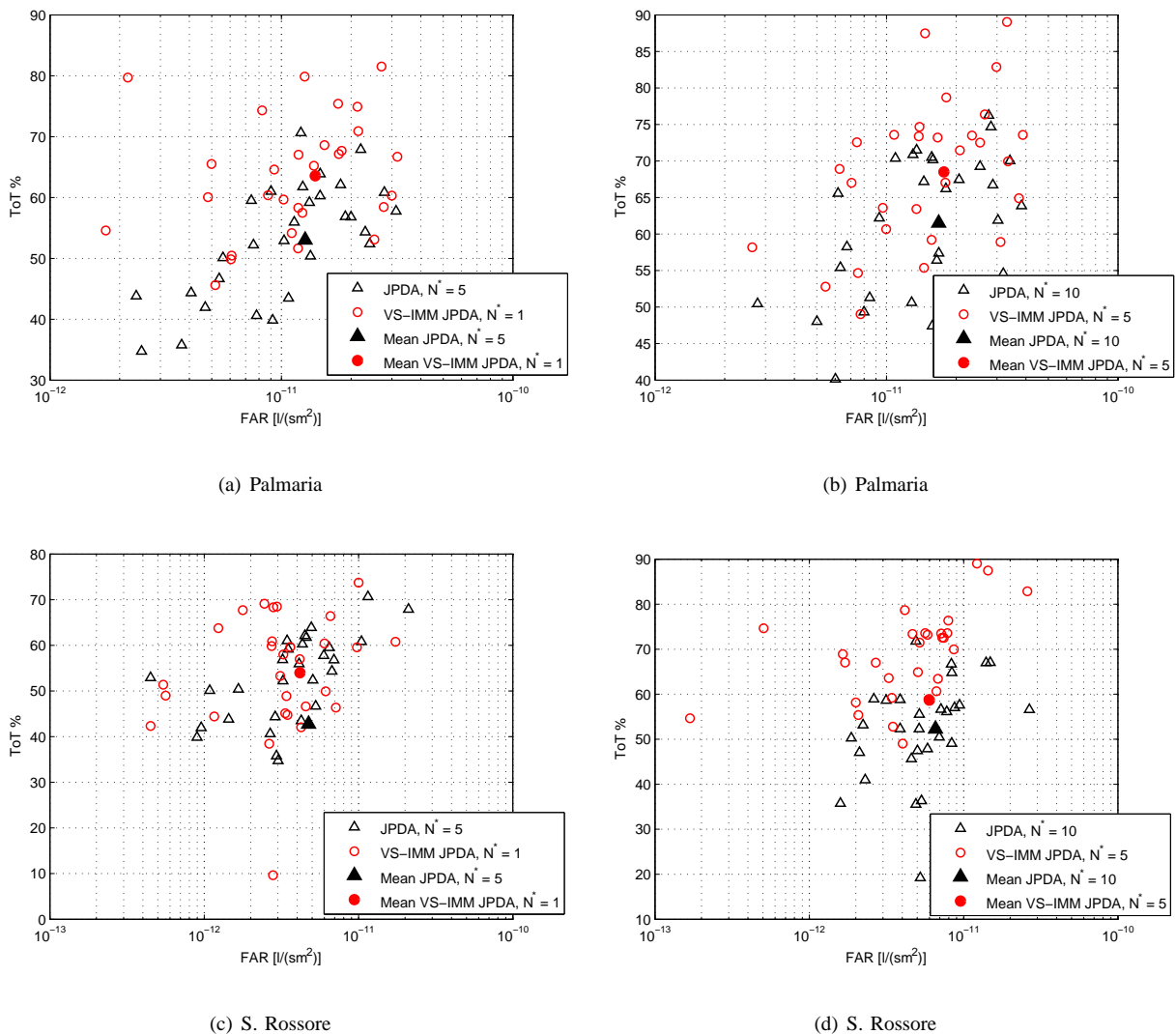


Fig. 11. Scatter plots represented the daily values of the couples ToT and FAR by varying N^* .

TABLE II

MEANS ON BOTH THE DATASETS FOR ToT AND FAR INDEXES.

(a) Palmaria					(b) S. Rossore				
N^*	JPDA		VS-IMM JPDA		N^*	JPDA		VS-IMM JPDA	
	$ToT\%$	$FAR [1/(sm^2)]$	$ToT\%$	$FAR [1/(sm^2)]$		$ToT\%$	$FAR [1/(sm^2)]$	$ToT\%$	$FAR [1/(sm^2)]$
1	36.04	$0.656 \cdot 10^{-11}$	63.03	$1.401 \cdot 10^{-11}$	1	28.24	$0.2262 \cdot 10^{-11}$	55.92	$0.4169 \cdot 10^{-11}$
5	52.84	$1.266 \cdot 10^{-11}$	68.11	$1.769 \cdot 10^{-11}$	5	42.65	$0.4735 \cdot 10^{-11}$	58.62	$0.5985 \cdot 10^{-11}$
10	61.62	$1.681 \cdot 10^{-11}$	69.55	$1.997 \cdot 10^{-11}$	10	52.79	$0.6563 \cdot 10^{-11}$	60.58	$0.7445 \cdot 10^{-11}$

The daily values are reported and the related means are indicated with full markers (see also Tab. II). It is easy to note that when the VS-IMM reaches the same FAR of the standard JPDA exhibits also a higher ToT . An improvement of 10% on the average is observed. In order to have a clearer plot, in Fig. 12 we report the convex hull of daily couples (ToT, FAR) .

Fig. 12 shows that the performance advantages are more evident in the low false alarm region. Furthermore, the improvements,

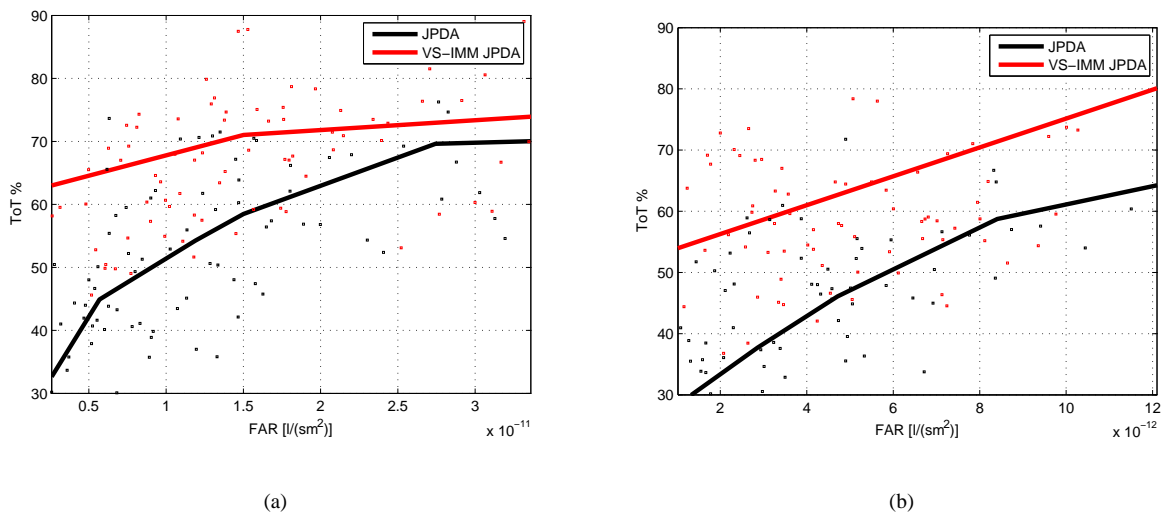


Fig. 12. ToT Vs. FAR varying N^* in the case of (a) Palmaria and (b) S. Rossore. Black and red little squares indicate the daily values for the standard JPDA and the VS-IMM JPDA, respectively.

TABLE III
DAILY MEANS AND STANDARD DEVIATIONS OF N^{TF} INDEX FOR BOTH THE DATASETS.

(a) Palmaria			(b) S. Rossore		
Date	JPDA (μ, σ)	VS-IMM JPDA (μ, σ)	Date	JPDA (μ, σ)	VS-IMM JPDA (μ, σ)
07/05	(1.18,0.40)	(1.29,0.49)	07/05	(1.13,0.35)	(1.13,0.35)
08/05	(1.62,0.83)	(1.40,0.65)	08/05	(1.67,0.99)	(1.37,0.56)
09/05	(1.67,1.17)	(1.36,0.49)	09/05	(1.82,1.33)	(1.41,0.80)
10/05	(1.86,1.28)	(1.45,0.89)	10/05	(1.31,0.60)	(1.12,0.34)
11/05	(1.67,1.24)	(1.60,1.12)	11/05	(1.38,0.87)	(1.23,0.83)
12/05	(1.65,0.71)	(1.43,0.60)	12/05	(1.64,1.15)	(1.36,0.63)
13/05	(1.89,1.19)	(1.59,0.89)	13/05	(1.62,0.96)	(1.31,0.60)
14/05	(1.56,0.93)	(1.16,0.47)	14/05	(1.60,0.83)	(1.43,0.65)
15/05	(1.52,0.82)	(1.17,0.39)	15/05	(2.11,1.76)	(1.32,0.58)
16/05	(1.77,1.41)	(1.39,0.79)	16/05	(1.78,1.44)	(1.58,0.84)
17/05	(1.52,1.29)	(1.16,0.50)	17/05	(1.48,0.59)	(1.35,0.57)
18/05	(1.42,0.69)	(1.29,0.69)	18/05	(1.13,0.35)	(1.00,0.00)
19/05	(1.66,0.94)	(1.23,0.53)	19/05	(1.27,0.46)	(1.07,0.26)
20/05	(1.33,0.82)	(1.50,0.58)	20/05	(1.00,0.00)	(1.00,0.00)
21/05	(1.43,0.77)	(1.00,0.00)	21/05	(1.62,0.51)	(1.33,0.49)
22/05	(1.69,1.16)	(1.14,0.36)	22/05	(1.69,0.87)	(1.35,0.61)
23/05	(1.96,1.51)	(1.46,0.90)	23/05	(1.79,0.80)	(1.64,0.74)
24/05	(1.57,0.79)	(1.26,0.45)	24/05	(1.44,0.63)	(1.50,0.65)
25/05	(1.75,1.07)	(1.39,0.70)	25/05	(1.72,1.07)	(1.50,1.03)
26/05	(1.62,0.95)	(1.27,0.56)	26/05	(2.56,1.98)	(2.24,1.82)
27/05	(1.75,1.36)	(1.50,0.88)	27/05	(1.87,1.54)	(1.56,0.96)
28/05	(1.62,1.01)	(1.27,0.46)	28/05	(1.47,0.64)	(1.20,0.41)
29/05	(1.50,1.05)	(1.37,0.88)	29/05	(1.65,1.11)	(1.35,0.79)
30/05	(1.83,1.62)	(1.33,0.96)	30/05	(1.50,0.89)	(1.44,0.63)
31/05	(1.61,1.46)	(1.24,0.56)	31/05	(1.56,0.73)	(1.37,0.52)
01/06	(1.45,0.94)	(1.13,0.35)	01/06	(1.40,0.52)	(1.30,0.48)
02/06	(1.65,1.23)	(1.18,0.39)	02/06	(1.83,1.15)	(1.78,1.11)
03/06	(1.90,1.72)	(1.28,0.70)	03/06	(1.24,0.75)	(1.19,0.54)
04/06	(1.75,1.29)	(1.37,0.56)	04/06	(1.86,1.46)	(1.50,0.94)

for the case of S. Rossore, are better than the ones for Palmaria, because of a worse capability of the radar in S. Rossore to detect the vessels, see also [6].

A further analysis is performed by exploiting the fragmentation index (N^{TF}). In Tab. III, the daily values of the means and the standard deviations of the N^{TF} calculated for each day with all the on-sea lane tracks are shown. The overall means

TABLE IV
DAILY ϵ^{pos} AND ϵ^{vel} FOR BOTH THE DATASETS.

(a) Palmaria					(b) S. Rossore				
Date	ϵ^{pos} [m]		ϵ^{vel} [m/s]		Date	ϵ^{pos} [m]		ϵ^{vel} [m/s]	
	JPDA	VS-IMM JPDA	JPDA	VS-IMM JPDA		JPDA	VS-IMM JPDA	JPDA	VS-IMM JPDA
07/05	736.3	751.4	0.70	0.68	07/05	1214.0	1155.4	1.74	1.66
08/05	617.1	623.4	1.12	0.91	08/05	886.7	880.9	1.07	0.87
09/05	670.1	688.9	0.98	0.91	09/05	929.6	987.9	0.92	0.70
10/05	518.6	568.4	1.04	0.98	10/05	1046.2	925.8	1.32	1.00
11/05	613.4	619.1	1.05	1.02	11/05	824.2	817.8	0.84	0.77
12/05	627.1	636.7	0.85	0.82	12/05	957.5	900.0	0.94	0.73
13/05	570.5	531.6	2.16	1.97	13/05	899.2	932.5	3.02	2.77
14/05	594.3	587.9	1.02	0.90	14/05	970.1	984.3	1.12	1.02
15/05	665.9	637.5	1.00	0.85	15/05	798.3	775.9	0.94	0.72
16/05	649.3	691.3	1.21	1.10	16/05	905.2	910.9	1.09	0.96
17/05	720.1	727.6	1.22	0.84	17/05	1208.5	1169.9	1.75	1.57
18/05	616.0	605.4	0.99	0.92	18/05	905.4	886.0	0.97	0.84
19/05	631.3	640.7	0.97	0.84	19/05	780.5	757.9	1.09	0.81
20/05	656.9	670.8	0.85	0.86	20/05	1257.3	1276.4	1.30	1.25
21/05	641.0	660.1	0.98	1.00	21/05	1024.2	1136.4	1.57	1.55
22/05	706.5	675.7	0.88	0.75	22/05	1103.5	1075.9	1.47	1.27
23/05	732.0	765.1	0.80	0.78	23/05	926.0	948.6	1.04	0.89
24/05	594.9	581.2	1.82	1.81	24/05	1102.6	1118.0	1.45	1.42
25/05	691.5	886.7	1.28	1.57	25/05	956.2	1001.5	1.34	1.12
26/05	713.5	734.2	1.16	1.10	26/05	892.7	816.2	1.00	0.79
27/05	492.1	513.2	1.18	0.93	27/05	1014.0	953.4	1.74	1.30
28/05	773.0	814.9	1.27	1.27	28/05	1006.8	1078.1	1.10	0.81
29/05	695.7	673.8	1.22	1.05	29/05	937.1	938.3	1.15	0.99
30/05	596.0	611.1	1.08	0.96	30/05	775.1	830.1	0.66	0.78
31/05	649.7	607.2	1.43	1.22	31/05	1146.9	990.4	1.44	0.90
01/06	624.9	687.9	1.18	1.27	01/06	1218.4	1238.0	1.41	1.22
02/06	792.5	801.1	1.02	0.96	02/06	1119.1	1079.3	1.91	1.74
03/06	618.2	575.6	1.21	0.86	03/06	732.9	809.0	1.72	1.90
04/06	707.3	672.4	1.38	1.15	04/06	1014.8	1002.9	1.08	0.86

for Palmaria are 1.63 for JPDA and 1.32 for the VS-IMM, and 1.59 and 1.38, respectively for S. Rossore. These outcomes confirm the capability of the KB-tracking to reduce the track fragmentation.

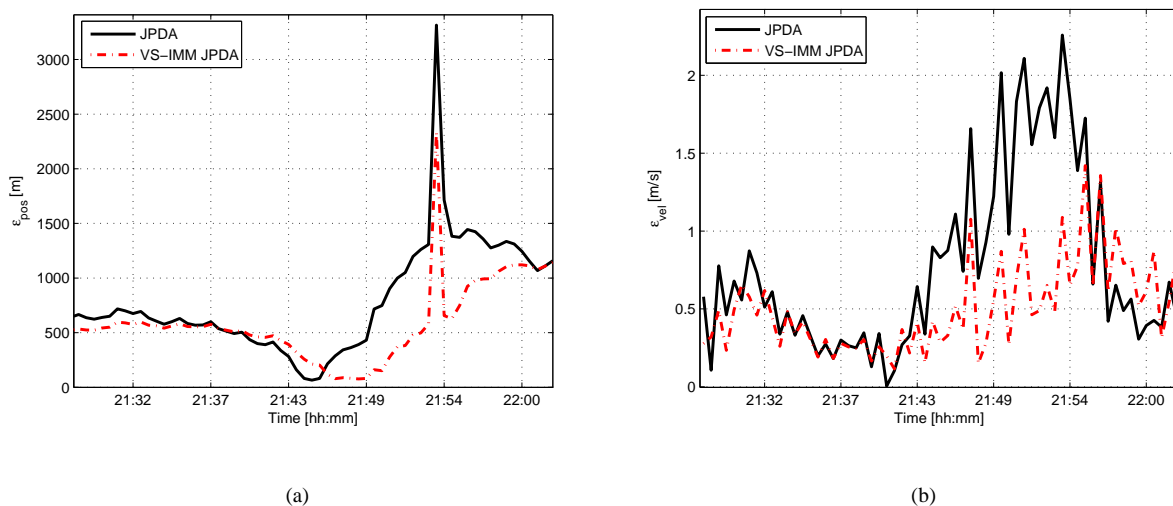


Fig. 13. (a) ϵ^{pos} and (b) ϵ^{vel} for an oil/chemical tanker with MMSI = 247104500 on May 28, 2009 recorded in the Palmaria dataset.

The last analysis is related to the RMSE of position and velocity. In Figs. 13 and 14, we report ϵ^{pos} and ϵ^{vel} indexes over time, using the VS-IMM JPDA and the standard JPDA. Two scenarios are shown in which an oil/chemical tanker and a container ship are observed by Palmaria and S. Rossore, respectively. We observe a sensible gain in terms of performance for

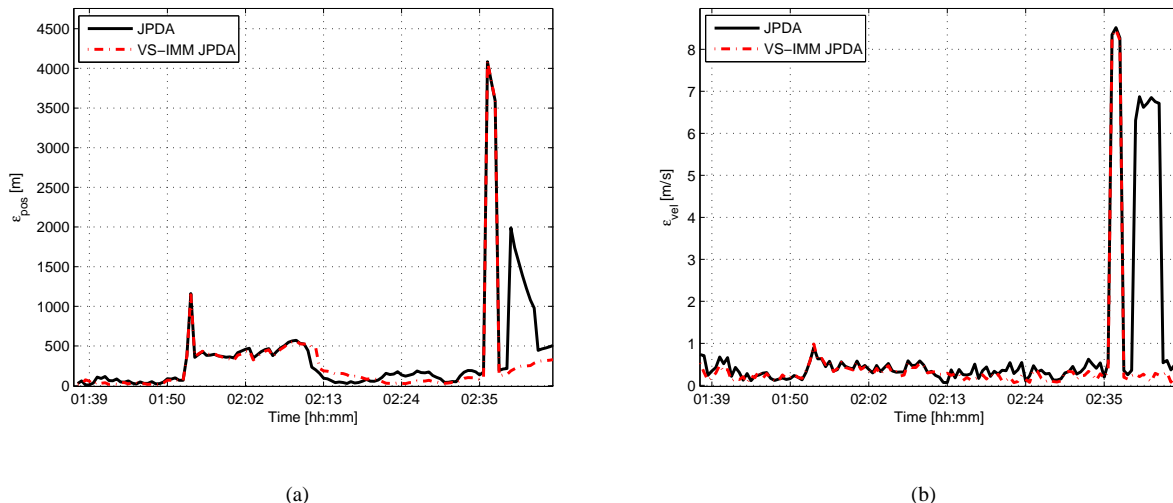


Fig. 14. (a) ϵ^{pos} and (b) ϵ^{vel} for a container ship with MMSI = 305272000 on May 8, 2009 recorded in the S. Rossore dataset.

both position and velocity, see for instance between 21:49 and 22:00 in Fig. 13 and from 02:35 to the end in Fig. 14.

Another phenomenon, related to the position RMSE index, is present. As already explained the standard JPDA exhibits a larger TF than the VS-IMM JPDA, thus it is likely that when there are few target-originated detections the JPDA breaks the track while the VS-IMM JPDA is still able to maintain it (using the on-sea lane logic). However, in this case, while the VS-IMM JPDA is maintaining the track an increasing error is exhibited (see Fig. 15(a) for the time interval from 04:35 to 04:46 and Fig. 15(c) between 06:04 and 06:16), with respect to the case in which there are several target-originated detections, and consequently it could be possible to reach an averaged error larger than the standard JPDA. An opposite effect is observed for the velocity. In this case, when a new track is initialized for the standard JPDA, the velocity starts from a quite noisy condition exhibiting, then, on the average a larger error with respect to the VS-IMM JPDA can be observed (see, for instance, Fig. 15(b) for the time interval from 05:10 to 05:41 and Fig. 15(d) between 06:04 and 06:18). Consequently, the propagation stage of the VS-IMM JPDA leads to an improvement of the ϵ^{vel} index.

In Tab. IV we report the daily values of ϵ^{pos} and ϵ^{vel} . The overall mean values on Palmaria of ϵ^{pos} are 652.3 [m] and 663.5 [m] for the JPDA and the VS-IMM, respectively, while, they are 984.6 [m] and 978.5 [m], respectively, in the case of S. Rossore. Practically, there is no appreciable advantage in terms of positioning error. Instead, by taking a look at ϵ^{vel} , the means are 1.14 [m/s] and 1.04 [m/s] for the standard JPDA and the VS-IMM, respectively, on the Palmaria dataset and 1.32 [m/s] and 1.15 [m/s] on S. Rossore's data. On the contrary, in this case, the performance advantages are evident (around 10%) for both the radars in Palmaria and S. Rossore.

V. CONCLUSIONS

Low-power/cost HFSW radars can be reliable long-range early-warning tools for maritime situational awareness applications.

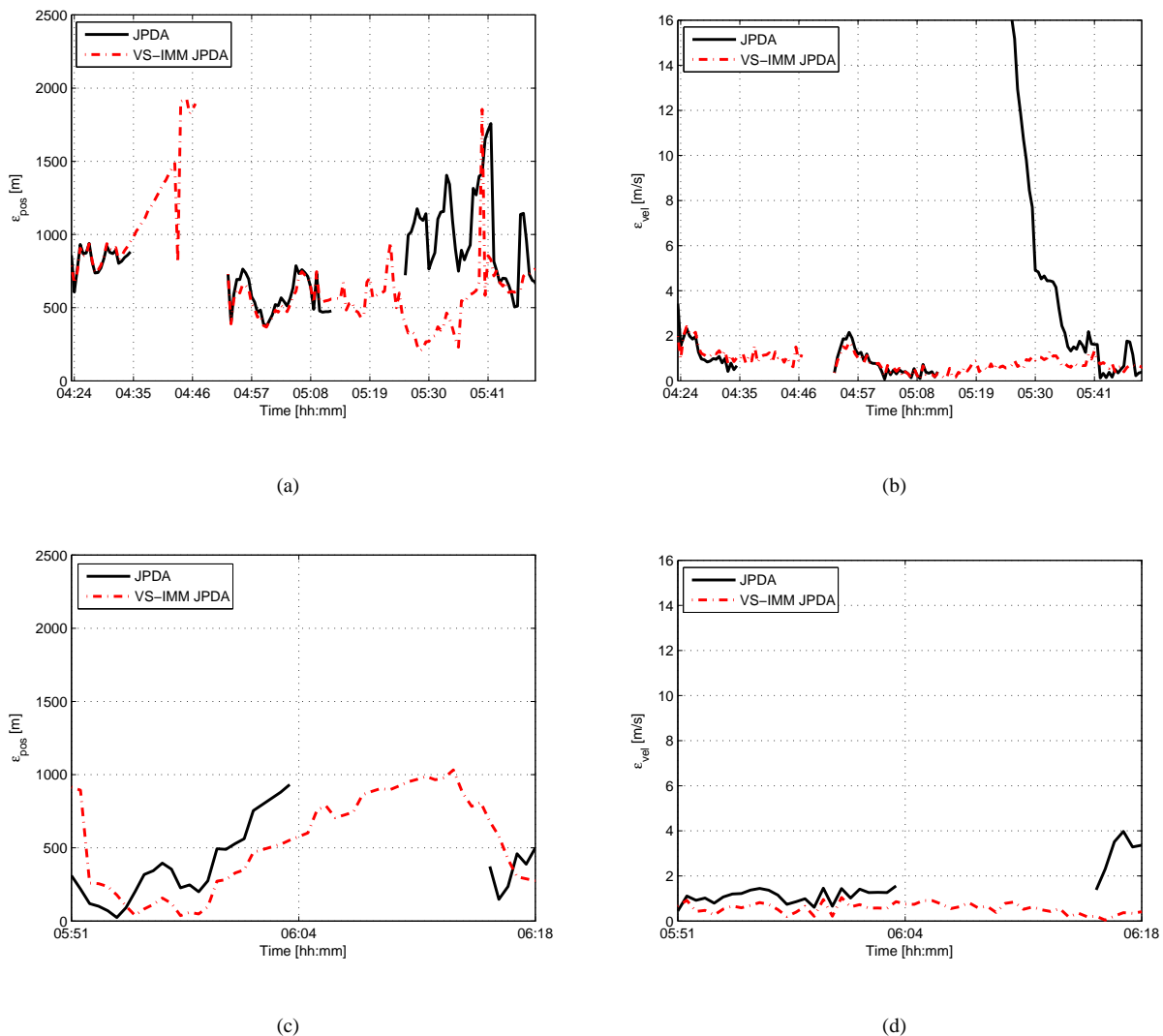


Fig. 15. ϵ^{pos} and ϵ^{vel} for two fragmented tracks on June 3, 2009 recorded in the Palmaria dataset. (a) and (b) show the errors for a passenger ship with MMSI = 247002300 between 04:24 and 05:50, while, (c) and (d) for an oil/chemical tanker with MMSI = 247088700 between 05:51 and 06:18.

In this paper, a self-adapting VS-IMM approach combined with a JPDA algorithm was presented for tracking ships with on-sea lane constrained motion in a multi-target environment. The targets can move on-sea lanes with a more constrained motion model than that in off-sea lane. In greater detail, motion uncertainties due to on-sea lane/off-sea lane motion and sea lane entry/exit conditions were handled using the above-mentioned estimator. Based on the sea lane map, obtained by the AIS historical information, and the predicted location of the target under track, the estimator mode sets were adjusted in real-time. In addition to the sea lane constraints, obscuration of the targets due to the radar synchronization and first order Bragg scattering reasons, was also handled within the VS-IMM framework.

Results on simulated and one-month real data (acquired by two different HFSW radars) collected during the NURC BP09 experimentation were presented and discussed. The advantages, in terms of, time-on-target and false alarm rate, track fragmentation and estimation errors, of the proposed VS-IMM JPDA with respect to the standard JPDA [6] were shown and

validated using AIS data as ground-truth. A significant improvement of the VS-IMM JPDA, in terms of system performance, were demonstrated. We have shown that there is an increment of the time-on-target for any fixed value of the false alarm rate. The increment is quite sensible in the region of low false alarm rate where can be over 30% for both the systems in Palmaria and S. Rossore. On the average we also obtain a reduction of the track fragmentation, about 20% and 13% for Palmaria and S. Rossore, respectively.

REFERENCES

- [1] D. E. Barrick and M. W. Evans, "Implementation of coastal current-mapping HF radar system," *NOAA*, no. 1, Jul. 1976.
- [2] R. J. Martin and M. J. Kearney, "Remote sea current sensing using HF radar: an autoregressive approach," *IEEE J. Ocean. Eng.*, vol. 22, no. 1, pp. 151–155, Jan. 1997.
- [3] K.-W. Gurgel and T. Schlick, "HF radar wave measurements in the presence of ship echoes - problems and solutions," in *Proc. of Oceans Europe*, Brest (France), Jun. 2005.
- [4] K.-W. Gurgel and G. Antonischki, "Remote sensing of surface currents and waves by the HF radar WERA," in *Proc. of the 7th IEEE Conf. on Electronic Eng. in Ocean.*, Southampton, UK, Jul. 1997.
- [5] S. Grosdidier, A. Baussard, and A. Khenchaf, "HFSW radar model: Simulation and measurement," *IEEE Trans. Geosci. Remote Sens.*, vol. 48, no. 9, pp. 3539–3549, Sep. 2010.
- [6] S. Maresca, P. Braca, J. Horstmann, and R. Grasso, "Maritime surveillance using multiple high-frequency surface-wave radars," *IEEE Trans. Geosci. Remote Sens.*, vol. 52, no. 8, pp. 5056–5071, Aug. 2014.
- [7] G. Capraro, A. Farina, H. Griffiths, and M. Wicks, "Knowledge-based radar signal and data processing: a tutorial review," *IEEE Signal Process. Mag.*, vol. 23, no. 1, pp. 18–29, Jan. 2006.
- [8] T. Kirubarajan, Y. Barshalom, K. Pattipati, and I. Kadar, "Ground target tracking with variable structure IMM estimator," *IEEE Trans. Aerosp. Electron. Syst.*, vol. 36, no. 1, pp. 26–46, Jan. 2000.
- [9] Y. Bar-Shalom, F. Daum, and J. Huang, "The probabilistic data association filter," *IEEE Control Syst. Mag.*, vol. 29, no. 6, pp. 82–100, Dec. 2009.
- [10] Y. Bar-Shalom, P. Willett, and X. Tian, *Tracking and Data Fusion: A Handbook of Algorithms*. Storrs, CT: YBS Publishing, Apr. 2011.
- [11] S. J. Julier and J. K. Uhlmann, "Unscented filtering and nonlinear estimation," *Proc. IEEE*, vol. 92, no. 3, pp. 401–422, Mar. 2004.
- [12] "NATO Alliance Maritime Strategy," *Official texts*, Mar. 2011.
- [13] A. Moreira, P. Prats-Iraola, M. Younis, G. Krieger, I. Hajnsek, and K. Papathanassiou, "A tutorial on synthetic aperture radar," *IEEE Geosci. Remote Sens. Mag.*, vol. 1, no. 1, pp. 6–43, March 2013.
- [14] K.-W. Gurgel, A. Dzvankovskaya, T. Pohlmann, T. Schlick, and E. Gill, "Simulation and detection of tsunami signatures in ocean surface currents measured by HF radar," *Ocean Dyn., Springer Berlin/Heidelberg*, vol. 61, no. 10, pp. 1495–1507, Oct. 2011.
- [15] K.-W. Gurgel, G. Antonischki, H.-H. Essen, and T. Schlick, "Wellen radar (WERA), a new ground-wave based HF radar for ocean remote sensing," *Coastal Eng.*, vol. 37, no. 3, pp. 219–234, Aug. 1999.
- [16] R. H. Khan, "Ocean-clutter model for high-frequency radar," *IEEE J. Ocean. Eng.*, vol. 16, no. 2, pp. 181–188, Apr. 1991.
- [17] S. Maresca, M. Greco, F. Gini, R. Grasso, S. Coraluppi, and N. Thomas, "The HF surface wave radar WERA. part I: Statistical analysis of recorded data," in *Proc. of the IEEE Radar Conf.*, Washington, USA, May 2010.
- [18] —, "The HF surface wave radar WERA. part II: Spectral analysis of recorded data," in *Proc. of the IEEE Radar Conf.*, Washington, USA, May 2010.

- [19] P. Braca, R. Grasso, M. Vespe, S. Maresca, and J. Horstmann, "Application of the JPDA-UKF to HFSW radars for maritime situational awareness," in *Proc. of the 15th Intern. Conf. on Inform. Fusion (FUSION)*, Singapore, Jul. 2012.
- [20] P. Braca, M. Vespe, S. Maresca, and J. Horstmann, "A novel approach to high frequency radar ship tracking exploiting aspect diversity," in *Proc. of the IEEE Intern. Geo. and Rem. Sens. Symp. (IGARSS)*, Munich, Germany, Jul. 2012.
- [21] S. Maresca, P. Braca, and J. Horstmann, "Data fusion performance of HFSWR systems for ship traffic monitoring," in *Proc. of the 16th Intern. Conf. on Inform. Fusion (FUSION)*, Istanbul, Jul. 2013.
- [22] —, "Detection, tracking and fusion of multiple HFSW radars for ship traffic surveillance: Experimental performance assessment," in *Proc. of the IEEE Intern. Geo. and Rem. Sens. Symp. (IGARSS)*, Melbourne, Jul. 2013.
- [23] A. Dzvonkovskaya, K.-W. Gurgel, H. Rohling, and T. Schlick, "Low power high frequency surface wave radar application for ship detection and tracking," in *Proc. of the IEEE Radar Conf.*, Vilnius, Lithuania, Sep. 2010.
- [24] K.-W. Gurgel, Y. Barbin, and T. Schlick, "Radio frequency interference suppression techniques in FMCW modulated HF radars," in *Proc. of Oceans 2007 Europe*, Aberdeen, Scotland, Jun. 2007.
- [25] A. Dzvonkovskaya and H. Rohling, "HF radar performance analysis based on AIS ship information," in *Proc. of the IEEE Radar Conf.*, Washington, USA, May 2010.
- [26] *Safety of Life at Sea (SOLAS) Convention*. Chapter V, Regulation 19.
- [27] M. Vespe, I. Visentini, K. Bryan, and P. Braca, "Unsupervised learning of maritime traffic patterns for anomaly detection," in *Data Fusion Target Tracking Conference (DF TT 2012): Algorithms Applications, 9th IET*, May 2012.
- [28] M. Vespe, G. Pallotta, I. Visentini, K. Bryan, and P. Braca, "Maritime anomaly detection based on historical trajectory mining," in *Proceedings of the NATO Port and Regional Maritime Security Symposium*, May 2012.
- [29] G. Pallotta, M. Vespe, and K. Bryan, "Vessel pattern knowledge discovery from AIS data: A framework for anomaly detection and route prediction," *Entropy*, vol. 15, no. 6, pp. 2218–2245, Jun. 2013.
- [30] G. Pallotta, S. Horn, P. Braca, and K. Bryan, "Context-enhanced vessel prediction based on Ornstein-Uhlenbeck processes using historical AIS traffic patterns: Real-world experimental results," in *Proc. of the 17th Intern. Conf. on Inform. Fusion (FUSION)*, Salamanca, Jul. 2014.
- [31] Z. Duan, C. Han, and X. R. Li, "Sequential nonlinear tracking filter with range-rate measurements in spherical coordinates," in *Proc. of the 7th International Conference on Information Fusion (FUSION)*, Stockholm, Sweden, Jun. 2004.
- [32] L. Bruno, P. Braca, J. Horstmann, and M. Vespe, "Experimental evaluation of the range-Doppler coupling on HF surface wave radars," *IEEE Geosci. Remote Sens. Lett.*, vol. 10, no. 4, pp. 850–854, Jul. 2013.
- [33] B. Chen and J. Tugnait, "Tracking of multiple maneuvering targets in clutter using IMM/JPDA filtering and fixed-lag smoothing," *ELSEVIER Automatica*, vol. 37, no. 2, pp. 239–249, Feb. 2001.